Upper mantle shear wave velocity structure in the southeastern United States from Rayleigh wave tomography

By
Dorran K. Howell

Advised by: Dr. Lara S. Wagner

Honors Thesis
Geological Sciences
University of North Carolina

April 14, 2014

Approved by:

Advisor: Dr. Lara S. Wagner

Abstract

Dorran K. Howell: Upper mantle shear wave velocity structure in the southeastern United States from Rayleigh wave tomography

(Under the direction of Lara S. Wagner)

We present a model of upper mantle shear wave velocity in the southeastern United States from Rayleigh Wave tomography that images the proposed Suwannee suture in southern Georgia. We use data that were recorded by the SESAME (the Southeastern Suture of the Appalachian Margin Experiment) seismic network and nearby EarthScope Transportable Array and permanent broadband stations. Preliminary results indicate a consistent depth to the lithosphere-asthenosphere boundary (LAB) across the Suwanee suture. We identify two zones of anomalously low shear wave velocity: one within the mantle lithosphere of the Suwannee Terrane that spans depths from the Moho to ~105km and a second zone beneath the southernmost Appalachians. These low velocities beneath Suwannee are likely due to the presence of water from subduction-related processes. This is consistent with Laurentia having been subducted beneath Suwannee Terrane during accretion (McBride and Nelson, 1988). The LAB depth is ambiguous for low velocity areas beneath the Appalachians, and further analysis is needed before this structure can be characterized.

Acknowledgements

I would like to thank my advisor, Dr. Lara S. Wagner, for her guidance and help throughout this project. I would like to thank Dr. Karen M. Fischer, Dr. Robert B. Hawman, and Sanja Knezevic Antonijevic for their technical guidance and help in the field. I would also like to thank all of the SESAME field crews that have aided in the collection of this data (and smashed a number of spiders in the process). Finally, I would like to thank NSF for providing the funding that made this project possible.

Table of Contents

List of Figures

List of Tables

1. Introduction

Previous studies in the southeastern United States have found that the basement rock of southern Georgia and Florida comprises an exotic terrane that was originally attached to Gondwana prior to the Alleghanian orogeny (e.g. Chowns and Williams 1983, Cramer 1971, Heatherington and Mueller 2003). The nature of the suture between these terranes is poorly understood. Some studies have argued for subduction of Laurentian lithosphere beneath Suwannee during accretion (e.g. Nelson and McBride, 1988), while others have argued for a transpressional margin (Mueller et al., 2013). Much of this uncertainty stems from a lack of data on deep lithospheric structures in this area. Our study provides new data on lithospheric mantle structure across the suture and provides new evidence supporting subduction during accretion.

2. Geologic Setting

2.1 The Suwannee Suture

Stratigraphic observations from boreholes in the Suwannee terrane reveal a sequence of relatively undeformed Paleozoic and Mesozoic sediments overlying a crystalline, Precambrian basement (e.g. Chowns and Williams, 1983). This sequence is different from the nearby Piedmont or coastal plains, which are a complex structural layering of crystalline Peri-Gondwanan rocks and overlying sediments (Thomas et al., 1989). Paleontological studies have shown that Paleozoic fossil assemblages in the Suwannee terrane do not match synchronic Laurentian deposits. Specifically, Cramer (1971) find that phytoplankton assemblages from Silurian deposits suggest that Florida arrived from a Gondwanan position during the Silurian assembly of Pangea. Pojeta et al. (1976) observe that Paleozoic Pelecypod assemblages in

Suwannee are similar to those found in Central Europe and conclude that Suwannee assemblages could potentially be correlated to those found in Central Europe, South America or Africa.

Initial geochemical studies suggested that Suwannee was derived from Africa. Detrital biotite $^{40}Ar/^{39}Ar$ ages from boreholes in the Suwannee terrane match ages of the Bové basin in West Africa, which has been suggested to correlate with parts of the Suwannee stratigraphic section (Dallmeyer, 1987). Furthermore, the Coyah granite of Guinea has been found to have a crystallization age of ~530Ma, which is similar to the $^{40}Ar/^{39}Ar$ age of the Osceola Granite in Florida (Dallmeyer et al., 1987).

More recent geochemical studies, however, have suggested that the Suwannee basement is derived from South American portions of Gondwana. Heatherington and Mueller (2003) examine igneous rocks from the Suwannee portion of the Central Atlantic Magmatic Province and find that related mafic intrusions were derived from a protolith that best matches lithospheric crust and mantle from South America. Heatherington and Mueller (2010) study the only known intrusions in Suwannee that pre-date rift volcanism (intrusions had ages of ~295Ma). Trace element analyses demonstrate that these intrusions were not subduction related and were likely related to post-orogenic volcanism following the Alleghanian. Ages of xenocrysts in the granites suggest that they are inclusions of Laurentian or South American country rock. Further analyses by Heatherington and Mueller (2010) show that crystallization age distributions for xenocryst zircons do not match ages for Laurentian tectonic events. They do however have overlapping ages with major orogenies in South America and, to a lesser extent, Africa. This suggests the Suwannee basement has a South American/Gondwanan origin (Heatherington and Mueller, 2010).

The lithospheric and surficial expression of the suture between Suwannee and Laurentia has been constrained by several studies. First identified by borehole data (Chowns and Williams, 1983), the Suwannee suture intersects the surface in southern Georgia (Figure 2.1). COCORP (The Consortium for Continental Reflection Profiling) created a series of seismic reflection profiles for this area in the 1980s. Reflection profiles reveal a series of southward dipping crustal reflectors in southern Georgia that extend to lower crustal depths. Reflectors are located north of local rift basins, suggesting that they are not related to rifting (Figure 2.2). These reflectors have been interpreted as the suture between Suwannee and Laurentia and suggest that Suwannee was thrust over the Laurentian continental block (Nelson et al., 1985a).

Further evidence that southward dipping reflectors in Georgia demarcate the Suwannee suture is the correlation between the location of these structures and the Brunswick magnetic anomaly. The Brunswick magnetic anomaly is a zone of low magnetism that crosses Georgia and extends into the Atlantic (Figure 2.3). A comparison of COCORP reflection data and magnetism showed that the Brunswick magnetic anomaly is centralized deep in the crust and is thus not related to material in local rift basins (McBride and Nelson, 1988). The dipping reflectors in the COCORP profiles occur along magnetized zones at the location of the Suwannee suture. McBride and Nelson (1988) propose three models for the Brunswick magnetic anomaly: A suture-zone ophiolite model where oceanic lithosphere overrides Laurentia; an obducted continental crust model where continental lithosphere overrides Laurentia; and a rift magmatic overprint model. They argue that the most likely model involves oceanic crust or mafic continental crust being thrust upward over Laurentian lithosphere (McBride and Nelson, 1988). Further modeling of the lower lithosphere and upper asthenosphere beneath the suture may better constrain both the cause of the Brunswick magnetic anomaly and mechanism of accretion of the Suwannee terrane.

2.2 Regional Tectonic History

Hatcher (2010) and Hibbard (2010) provide detailed summaries of regional tectonics from the Proterozoic into the Cenozoic. The earliest records of large-scale tectonics along the eastern margin of Laurentia start in the mid to late Proterozoic with the Grenville orogeny. The Grenville orogeny coincides with the formation of the supercontinent Rodinia. Compressional tectonics during this time caused widespread regional metamorphism and extensive uplift along the eastern section of Laurentia (Hatcher 2010).

The super-continent Rodinia broke-up at ~750Ma, starting the Wilson cycle that would eventually form the Appalachians. Rifting proceeded in two phases: an initial period of failed rifting starting at ~735Ma that produced intrusives throughout the Laurentian craton and a final period of successful rifting along the Laurentian margin starting at ~565Ma which opened the Iapetus ocean (Hatcher 2010).

The rifted Laurentian margin existed as a passive margin until into the Ordovician. As the Wilson cycle continued, subduction of Iapetan oceanic lithosphere beneath Gondwana created a series of volcanic arcs between the two supercontinents. Starting at ~450-400Ma these peri-Gondwanan terranes started to collide with and accrete to the eastern margin of Laurentia, collectively resulting in two major orogenies: the Taconic at ~450Ma and the Acadian at ~350Ma (ages for these events vary with location along the margin). Collision of arc terranes with Laurentian craton caused extensive uplift in the Appalachians as well as regional metamorphism (Hatcher 2010). Compression during this time was partially accommodated on reactivated Grenville-age faults (Hatcher, 2010). While there are a number of peri-Gondwanan terranes associated with the Taconic and Acadian orogenies, our study area is primarily focused on the Suwannee terrane and its relation to neighboring Laurentian lithosphere (Figure 2.1) (Hatcher, 2010).

Eastern Laurentia experienced a transitional period following the Acadian orogeny until the early Carboniferous when Gondwana and Laurentia started to collide, causing the Alleghanian orogeny. Continental collision during the Alleghanian may have occurred as a "zippered" pattern, starting in the north and progressively closing to the south along dextral transpressional faults (Hatcher, 2010; Peavy et al., 2004; Engelder and Whitaker, 2006; Hatcher, 2001). These motions are believed to have started with a major dextral component and have transitioned to a more dominant compressional component (Hatcher, 2010). This notion is supported by analyses of deformational structures in both the Piedmont and Blue Ridge (Secor et al., 1986). Still, it is important to note that some research suggests an earlier date for collision in the southern section and a somewhat more direct pattern of collision. Hibbard (2010) suggests that magmatism in southern Laurentia may be associated with preliminary interactions with the Gondwanan Suwannee terrane occurring somewhat earlier than commonly estimated dates for the Alleghanian orogeny. Such interactions would be analogous to the Famennian event in northern Laurentia and would indicate a less dextral direction of collision (Hibbard, 2010). The Alleghanian orogeny culminated with the formation of Pangea during the late Permian (Hatcher, 2010).

Deformation from the Alleghanian orogeny caused uplift along the Neoproterozoic Laurentian margin and formed a foreland fold and thrust belt (Hatcher, 2010). Deformation in the Appalachians may be categorized as thin-skinned (Cook and Vasudevan, 2006). Signals of deformation appear in both the Piedmont and Blue Ridge, suggesting that the Appalachian décollement extends beneath the Piedmont (Secor et al., 1986). This notion has been confirmed by the reprocessing of seismic reflection data from the region (Cook and Vasudevan, 2006). Other studies have reinforced this point by identifying eastward dipping seismic reflectors along the eastern margin of the Blue Ridge, which are associated with the Laurentian margin (Peavy et al., 2004). It is also noted that crustal thickness is greatest beneath the Appalachians and decreases eastward towards the Atlantic (Peavy et al., 2004). Overall, both the Piedmont and Blue Ridge are estimated to have been thrust >175km to the northwest (Secor et al., 1986; Cook et al., 1979).

During the early Jurassic, the regional compressional regime transitioned to an extensional one. Initial extension was accommodated by continental lithosphere near the Laurentian-Gondwanan boundary, forming rift basins across the eastern Laurentian margin (Hatcher, 2010). The largest of these are found in present day Georgia and northern Florida, and include the South Georgia rift basin – a prominent lithospheric structure in our study area (Figures 2.1-2.2) (McBride et al., 1987).

Continental rifting continued until ~200Ma when the locus of extension abruptly shifted to what may be considered the present day continental margin (Hynes 1990). This shift is demarcated by a series of igneous intrusives and flood basalts called the Central Atlantic Magmatic Province (CAMP) (Nomade et al, 2006). Rifting in the southeastern section of the Laurentia-Gondwana boundary occurred seaward of the Suwannee terrane, which had been accreted to Laurentia along the Suwannee suture during the Alleghanian (Hatcher, 2010; Hibbard, 2010).

The South Georgia rift basin was characterized by a series of studies using COCORP seismic reflection data. The basin is a series of disjointed half-grabens with the largest section having a width of ~110km and a maximum basin fill of ~6km. The structure of the basin can be summarized as the following: a lower section of thicker and tilted sedimentary units; a layer of Jurassic basalts (CAMP); and an upper section of thinner, less faulted stratigraphy. These sections are reflective of different phases of rifting, with the lower units representing failed rifting and the upper units representing basin fill following the transition to oceanic rifting (McBride et al., 1987).

A passive margin developed along the eastern margin of Laurentia as rifting continued at the oceanic divergent boundary (the present day Mid-Atlantic Ridge). A lack of regional tectonic events has allowed for the development of a broad coastal plain along the Atlantic margin of Laurentia where sediments from the Appalachians are deposited in passive margin basins. Consequently, a record of regional tectonics, especially late-stage rifting, has been preserved along eastern Laurentia (Thomas, 2006).

3. Data Collection and Processing

For this study, we collected data from a total of 213 stations associated with two broadband seismic deployments: SESAME (Southeastern Suture of the Appalachian Margin Experiment), which comprises 85 EarthScope Flexible Array stations, and 128 local EarthScope Transportable Array stations (Figure 3.1). Events were chosen with magnitudes ≥ 6.2 and depths ≤ 100km to help ensure clear Rayleigh wave arrivals. Events ranged in date from May 2012 to May 2014. We found a total of ~50 events based on these criteria, though this number was later reduced to 32 (Figure 3.2) based on signal quality issues.

We used vertical component seismograms to observe arrivals of fundamental mode Rayleigh waves. We normalized the data for instrument response using the pole/zero data for each instrument type that was provided by IRIS (Incorporated Research Institutions for Seismology), using the Streckeisen STS-2 sensor as a standard. Waveforms were filtered for 16 frequency ranges, spanning 2-50 mHz and centered on periods ranging from 22.2 to 143s, using a band-pass filter in SAC (Seismic Analysis Code). Input parameters for filtering were set to a Butterworth filter type with 4 poles and 2 passes, resulting in zero-phase shift. We used a varying bandwidth for filter windows centered on different periods: 7 mHz for periods of 143 to 100s; 8mHz for periods of 91 and 77s, and 10mHz for periods of 66.7 to 22.2s. We visually inspected filtered seismograms for each event and removed stations having obvious sensor issues or signal-to-noise ratios less than 3 to 1. We also removed events that lacked clear Rayleigh wave arrivals from the dataset.

Time windows were cut for Rayleigh wave phases in order to distinguish them from other arrivals apparent on the filtered seismograms. We manually selected event windows for the first and last arrivals of each event and extrapolated to intermediate arrivals using a simple linear distance relationship and constant window length for a single period/event pair. We also utilized a minimum length of three times a respective period in order to avoid underestimating window size. Cut windows were then tapered at each end using a Hanning taper (Figure 3.3).

4. Methods

4.1 Phase Velocity Model

We utilize the two-plane wave method of Forsyth and Li (2005) and the finite frequency kernels of Yang and Forsyth (2006) to model Rayleigh wave phase velocities. Heterogeneous earth structure can cause multipathing of incoming energy as well as deviations from projected great circle path. The two-plane wave method accounts for these factors by modeling an incoming wave field as two plane waves arriving from different back azimuths. The phase and amplitude of an arrival at grid nodes across a study area are considered as a function of the constructive and destructive interference of the two incident waves (Forsyth and Li, 2005). For the first step in this calculation, we best fit the phase, amplitude, and backazimuth for each of the two plane waves using a simulated annealing method. We then use these parameters to calculate predicted amplitude and phase at each station in our study area. Differences between these sets of values are input into our inversion (Wagner et al., 2010).

Our inversion includes the finite frequency kernels of Yang and Forsyth (2006). These 2D sensitivity kernels have been shown to more accurately reflect the sensitivity of a given phase to velocity deviations than simple Gaussian sensitivity kernels (Li, 2011). Finite frequency kernels address scattering along a ray path as well as the fact that ray theory assumes infinitely high frequency (i.e. infinitely thin ray path), an assumption that has limitations when considering longer periods. Consequently, finite frequency kernels do a significantly better job of imaging finer scale velocity structures (Yang and Forsyth, 2006).

Our model starts with an initial condition of phase velocities calculated using P and S wave velocities from IASP91 (Kennett and Engdahl, 1991). We calculate a predicted phase and amplitude for each of the two plane waves for each station. Grid nodes are spaced in 0.33° increments over a 12° latitude by 12° longitude area, centered at 31°, -83.1296°. A total of 1296 grid nodes are used. Our inversion iteratively best fits perturbations in phase velocity for each period and grid node to reduce the difference between observed and predicted phase and amplitude. A total of 10 iterations were performed in this part of the inversion. We include damping parameters of 0.1 to promote stability of the model and also account for geometrical spreading and anelastic attenuation.

4.2 Shear Wave Velocity Model

The first step in calculating shear wave velocities is the designation of a starting model. Here, we start with an initial model from IASP91 (Kennett and Engdahl, 1991). We then adjust the depth of the Moho using a combination of data, including the Crust 1.0 model (Laske et al., 2013), and data from Parker et al. (2013) and Wagner et al. (2012) (Figure 4.1). We then designate a set of horizontal layers that are allowed to vary in shear wave velocity during the inversion (Table 4.1). Since Rayleigh waves are primarily sensitive to shear wave velocity at the sub-crustal depths of interest in this study (Weeraratne et al., 2003), we only focus on inverting for shear wave velocity and set the P to S wave velocity ratio to a fixed value of 1.73 in the crust and 1.79 in the mantle.

After developing our starting model, we calculate the predicted phase and amplitude of Rayleigh wave arrivals on a grid of 0.1° increments across our study area (the same map region as for the phase inversion). We then iteratively solve for perturbations in our starting velocity model that allow it to best fit our calculated phase velocity model. A velocity damping of 1 standard deviation is used for this inversion, which is performed for a total of 5 iterations. The output of this inversion is a 3-dimensional grid along 0.1° increments that contain values for shear wave velocities and percent deviation of velocity from our starting model.

5. Results

5.1 Phase Velocities

Maps of 1-dimensional phase velocities are shown in Figure 5.1a. Standard deviation values for each period are shown in Figure 5.1b. Resolution is greatly diminished in offshore areas for which we have no data and to the northeast where the Transportable Array stations arrived later (Figure 3.1).

One of the more notable features in the Suwannee suture area is the zone of lower phase velocities that trends approximately E-W at 33 s period (Figure 5.1a). While not entirely clear at all periods, this feature continues to be distinct at 45 s, 91 s, and 111 s. Surrounding this feature at 33 s period are broad regions of higher phase velocity to the north and south. While unclear at all periods, this structure of two zones of high velocity separated by an E-W trending low also appears across a great range of depths in shear wave velocities (Figure 5.2).

Another region of low phase velocities occurs at approximately 31°, -82°. This discrete region is distinct in phase maps for periods of 33 s, 40 s, 58 s, 66 s, and 100 s. This feature appears to be connected with the broader low velocity region for 50 s, 91 s, 111 s, 125 s, and 143 s, and the two structures may be related. A third zone of lower phase velocities also occurs beneath the Appalachians for periods ranging from 33 s-58 s. All three of these phase velocity structures have analogies in cross sections of shear wave velocity, which will be discussed below.

5.2 Shear Wave Velocities

Maps of shear wave velocities for depths ranging from 65-165 km reveal a predominant set of negative anomalies trending roughly E-NE in this area that are defined by ~3-4% dVs and absolute shear wave velocities of around 4.4 km/s (Figure 5.2). This feature is visible from the base of our model crust to depths of ~105 km (Figure 5.2). At around 145 km, most of the study area has a negative velocity anomaly, a trend that continues to spread and intensify with depth.

A sub-crustal gap in relative high shear velocities near the southern extent of the SESAME experiment is visible in our absolute shear wave velocity cross sections (Figures 5.3 to 5.8). Shear wave velocities of 4.5 km/s are fairly typical of upper mantle material in our starting earth model (Kennett and Engdahl, 1991). Velocities greater than this value, such as contours for

4.6 and 4.7 km/s, indicate relatively high velocities compared to our initial model. Similarly, values lower than around 4.4 km/s indicate relative low velocities (Kennett and Engdahl, 1991). On the western SESAME line (cross section A), higher velocities tend to have a relatively consistent maximum depth for section locations of 200-500 km along strike (Figure 5.4). There is a gap with a general lack of high velocities moving southward, until velocities of > 4.5 km/s return from ~650-775 km along strike (coincident with the land-ocean boundary). A relative low sub-crustal velocity zone appears above high velocity zones starting at around 400km along strike and persists for the rest of the southernmost section. This area of low velocities is connected to the other low velocity region at ~500-650 km along strike. There also appears to be a southward dipping structure occurring at ~400 km along strike in cross section A. Southward dipping mantle structures appear to occur in the same area that Nelson et al. (1985a) observe southward dipping crustal structures (Figure 5.4).

Cross section B (Figure 5.5) lacks regions of high velocity comparable in size to those in cross section A (Figure 5.4). Higher velocities appear beneath the crust along the beginning of the section line and appear along the last ~150km along strike. A zone of relative lows is visible above relative highs in the easternmost length of the section, much like that in our section along the western SESAME line (Figure 5.4).

Cross section C follows the eastern line of stations in the SESAME array (Figure 5.6). In this section, we see extensive relative low velocities occurring over high velocities from ~450km along strike southward. The deep gap in high velocities to the west is less clear in cross section C and appears to fade moving eastward (Figures 5.4 and 5.6). Because we lack data in the southwestern portions of our study area, we are not able to confidently project structures to the west of our array. Section D crosses the region just north of the Suwannee suture (Figures 2.1

and 5.8). There is little variation in the occurrence of high velocities across this line of section, indicating a more regular structure.

In cross section E, we observe relatively high shear velocities in the mantle for depths ranging from ~50-130 km (Figure 5.8). Below this, velocities are relatively low. Similar to cross sections farther north, this section shows a layer of relatively low velocities above relative highs. While poor station density this far south may limit our constraints on this shallow low velocity structure, it also occurs in areas with robust station density. The consistency of our results suggests that these anomalies are real and not related to diminished resolution. Crustal thicknesses for this region are poorly constrained, and we were limited to using Crust1.0 (Laske et al., 2013) crustal thickness estimates for our inversion's starting model. Crust1.0 is a continent-wide model of crustal thickness (Laske et al., 2013) and may not accurately reflect local crustal thickness. Anomalous subcrustal low velocities could be partially caused by a deeper Moho than what our starting model was parameterized with. However, these low velocities appear to vary regionally and be connected to the deeper zone of lower velocities visible at 500-650 km AS in cross section A (Figure 5.4). It is more likely that sub crustal low velocities are related to mantle lithospheric structure than a poorly constrained Moho.

We also observe a region of low velocities in northern Georgia centered around 34.9°, -83.3° (Figure 5.2). The low velocity zone appears in cross sections of absolute shear velocity and extends from the Moho to around ~125km depth (Figure 5.4). Relatively high mantle shear velocities of 4.5-4.6 km/s re-appear below this low zone. A similar decrease in crustal P-wave velocity north of the Suwannee suture has been observed in preliminary Pn body wave studies (Figure 5.9) (Julia MacDougall, personal communication, April 11, 2014)

In summary, we observe three major velocity structures: generally consistent subcrustal high velocities across much of southern Georgia and northern Florida; a zone of relative low velocities in mantle lithosphere trending roughly E-W at ~31° latitude; and another low velocity zone that is centered beneath the southern Appalachians.

6. Discussion

6.1 Lithospheric Thickness

The contrast between high viscosity lithosphere and lower viscosity asthenosphere is a fundamental concept to the theory of plate tectonics (O'Reilly and Griffin, 2010). It has been proposed that the transition varies as a function of several variables, including: thermal gradient, partial melt content, mineral grain size, chemical composition, and water content (Fischer et al., 2010). For continental regions, the lithosphere-asthenosphere boundary (LAB) primarily results from a change in chemical composition and water content (Fischer et al., 2010). The LAB generally ranges in depth from ~150-200km beneath cratons to shallower in areas with more recent tectonism (O'Reilly and Griffith 2010, Fischer et al. 2010, Abt et al. 2010, Ford et al. 2010).

To better approximate LAB depth we perform a simple calculation on our model's 1-D shear wave velocity profiles. We first calculate the depth range of the maximum negative gradient in shear wave velocity below an upper mantle high–velocity "lid" (e.g. Eaton et al., 2009). We then estimate the LAB as the midpoint of depths associated with the maximum negative gradient (See Figure 6.2) (e.g. Eaton et al., 2009). This technique has been demonstrated by studies such as Palomeras et al. (2014) and Weeraratne et al. (2003) and is summarized by Eaton et al. (2009). Examples of shear wave velocity profiles and LAB depths for areas around the Suwannee suture region are shown below in Figures 6.1-6.5. It is important to note that this calculation is performed using our model shear wave velocity profiles, which have been observed to vary with small changes to input parameters. Furthermore, shear velocity profiles can be equally fitted to surface wave data using either a short and rapid gradient or a long and gradual one (Eaton et al., 2009). As such, we limit our focus to LAB estimations in areas near the Suwannee suture that have relatively high station density. The LAB often occurs over a range of depths rather than at a discrete depth (Fischer et al, 2010). Thus, our depths are only a rough estimation of the LAB.

Estimated LAB depths correspond with both our shear velocity map and our cross section estimates. The LAB appears between contours for 4.5 and 4.4 km/s absolute shear velocities at depths greater than 100 km. These contours express LAB geometry across the Suwannee suture. The LAB is continuous across the area McBride and Nelson (1988) identify as the Suwannee suture (Figures 6.1-6.2 and 6.5). The LAB appears at depths of ~130-150km across the Suwannee suture area. Estimated LAB depths vary sporadically throughout the study area, sometimes even as much as ~20-30 km (Figure 6.5). This is expected, given the transitory nature of the LAB (Fischer et al., 2010) and the large range of acceptable depths for an individual LAB calculation. Interestingly, our estimated values differ from those of a continent-wide study of upper mantle discontinuities for North America by Abt et al., 2010. Abt et al. (2010) observe a decrease in velocity with depth between 90 and 100 km below Georgia that they attribute to the LAB. This discrepancy may be the result of a negative velocity gradient for depths ~75-90 km that is visible in one of our shear velocity profiles (Figure 6.3). This low velocity zone may correspond to the negative Sp phase Abt et al. (2010) attribute to the LAB. Our results suggest that the LAB occurs deeper at ~125-150km depth. The negative phase Abt et al. (2010) observe may be attributed to a low velocity zone within the lithospheric mantle. Our LAB estimate appears to be consistent with general ranges for continental lithosphere and regions affected by Phanerozoic orogenesis (Fischer et al., 2010).

6.2 Interpretation of Low Velocity Zones

The zones of relative low subcrustal phase and shear velocity in northern Florida/Georgia (Figures 5.1 and 5.2) are the most prominent velocity features in the Suwannee suture region. What defines these features? How may they relate to other regional tectonic features? A variety of hypotheses may be examined to answer these questions. Here, we focus on the characterization of these features and their relation to the two most recent major tectonic events to occur in this area: the Alleghanian orogeny and Mesozoic continental rifting (Hatcher, 2010).

Low shear wave velocities in the upper mantle may be caused by a variety of factors, and each should be considered when interpreting velocity structures. Partial melt fraction, olivine grain size, water content, and chemical composition all may contribute to variations in shear velocity (Fischer et al., 2010).

Partial melting is unlikely be a factor because there is no evidence for a high geothermal gradient in this area. Surface heat flux values for this area place heat flux at or below average for continental lithosphere (Blackwell et al., 1991) (Figure 6.6). Without a high thermal gradient, it is unlikely that temperatures at the depths we see these lows at (from ~50 to 105 km) are high enough to cause partial melting (Winter, 2010).

Olivine grain size may have a role in affecting seismic wave velocity differences in the mantle (Faul and Jackson 2005, Jackson et al. 2002). Jackson et al. (2002) found that smaller grain sizes tend to be associated with greater attenuation and lower velocities. Still, grain size tends to only be able to account for more gradual shifts in seismic velocities (Fischer et al., 2010). While grain size may be affecting the velocity contrast we see along northern FL, it is difficult to fit the sharp lateral gradient we observe (Figure 5.2) with only lateral variations in grain size.

The remaining factors to consider include water content and chemical composition. It has been suggested that observed crustal structures in this area may indicate that Laurentia subducted beneath Suwannee (e.g. McBride and Nelson, 1988). An increase in water content within the lithospheric mantle is possible if subduction occurred during the accretion of Suwannee. Increased percentages of hydrous phases in overriding lithosphere have been observed in a variety of subduction settings (e.g. Peacock, 1990). The subduction of oceanic and/or Laurentian lithosphere as Laurentia and Suwannee converged could provide a source for water in the lithospheric mantle (Winter, 2010). Hydrous, subduction-related intrusions could potentially reduce seismic wave velocities where they were intruded into generally de-hydrated mantle lithosphere (Fischer et al. 2010, Karato 2003, Karato and Jung, 1998).

A difference in chemical composition between the relative-low zone and surrounding mantle is another potential explanation. Relatively felsic, crustal rocks tend to have lower seismic wave velocities than ultramafic, mantle rocks (e.g. Christensen, 1978). However, it is not likely that relatively felsic rock is causing low velocities in the mantle lithosphere. While felsic magma may be found in the crust at convergent boundaries (Winter, 2010), one would not expect to find significant felsic melt in the mantle. In subduction zones, it is the dehydration of subducting crust that drives melting of asthenosphere and overriding lithosphere (Winter, 2010). Water released from dehydration tends to flow upward due to density differences with surrounding material, so it is less likely that subducted lithosphere will melt because of a wet solidus (Winter, 2010).

Fertile, asthenospheric rocks, with increased percentages of pyroxenes, tend to have lower seismic wave velocities than those in the lithospheric mantle (Fischer et al., 2010). However, the relative contribution of fertility to shear wave velocities is debatable. Some have argued for contributions of up to ~2.5% variation between fertile and depleted mantle rock (Lee, 2003). Others have argued for < 1% effect (Schutt and Lesher, 2006). It is not clear that a variation in fertility would create the sharp lateral velocity gradient that we observe.

6.3 Tectonic Implications

The observed low velocity zone has spatial patterns that correspond with regional tectonic features. The overall trend of this feature roughly follows local rift basins, but there are significant areas where the two do not spatially match. For example, rift basins extend farther to the north than our observed low velocity zone (Figures 2.2 and 5.2). Emplacement of fertile, asthenospheric peridotite in mantle lithosphere could possibly occur as a result of convection and upwelling (Drury et al., 2001). Mesozoic continental rifting could cause upwelling and emplacement of asthenospheric material in this area (Storey, 1995). Still, the debatable influence of fertility on seismic velocity (Schutt and Lesher, 2006) suggests that the high lateral velocity gradient we observe is not the result of differences in fertility.

Subduction of the Laurentian craton beneath Suwannee provides a better explanation of the observed lithospheric low velocity anomaly. Dehydration of subducted Laurentian continental and/or oceanic lithosphere could produce hydrous melt. (Winter, 2010). Magmas derived from this melt would be expected to intrude into the overriding plate, in this case Suwannee (Winter, 2010). In our model, the low velocity anomaly is constrained to regions within Suwannee. (Figures 2.1 and 5.2). Furthermore, we observe a southward dipping structure in cross section A that appears to coincide with the Suwannee suture (Figure 5.4). Relatively hydrous intrusions into Suwannee and southward dipping structures would fit a subducted-Laurentian model. The lack of observed subduction volcanics in Suwannee has been used to argue against subduction models (e.g. Mueller et al., 2013). While there is a lack of a robust record of late-Paleozoic intrusions near our low velocity zone, basement rock studies conducted on this area are limited in number (e.g. Chowns and Williams, 1983). Studying this area is further complicated because Mesozoic rifting and volcanism have influenced much of the crustal structure. A number of rift-related mafic intrusions have been identified in the crust on both sides of the Suwannee suture (e.g. Daniels et al. 1983, Chowns and Williams 1983). The dense coverage of rift structures and intrusions in this area may make identification of crustal Alleghanian intrusives more difficult. However, it appears that low velocities in Suwannee mantle lithosphere are related to Alleghanian (i.e. subduction) tectonics and not Mesozoic rifting.

Our results also address the hypothesis that the Suwannee suture is a transpressional margin that lacked a substantial subduction component (Mueller et al., 2013). One would not expect hydrous phases in the mantle lithosphere without a subduction component (Winter, 2010). Additionally, a margin with a greater transform component would not be associated with mantle upwelling that could emplace fertile rock into the lithosphere (e.g. Morgan and Forsyth, 1988). A model where the Suwannee suture is a transpressional margin does not fit our results.

Lithospheric delamination during the accretion of Suwannee and later continental rifting was previously theorized but has yet to be supported (e.g. Sacks and Secor, 1995). One of the goals of the SESAME experiment is to determine the validity of this theory by constraining lithospheric structure in the area. Lithospheric delamination is generally defined as the detachment of relatively dense lithosphere into lower density asthenosphere (Moore and Wiltschko, 2004). Sacks and Secor (1995) propose that a lithospheric delamination model fits structural and geochronological data for the southern Appalachians. They propose that southward-subducted oceanic lithosphere delaminated; causing decreased lithospheric thickness (Sacks and Secor, 1995). Moore and Wiltschko (2004) also show varying lithospheric thickness along convergent plate boundaries where delamination has occurred. The general consistency of our calculated LAB depth across the suture zone (Figures 6.2 and 6.5) suggests that delamination did not occur in this area.

The zone of low mantle shear velocities in the northern portions of the SESAME experiment is less well understood. Low velocities are distinct from the Moho to ~120 km depth. This feature appears to occur within the lithospheric mantle because a positive shear velocity gradient exists below it (Figure 6.4). However, shear wave profiles and LAB estimates for this location are fairly ambiguous (Figure 6.4). Interestingly, this zone occurs in the general location of the Blue Ridge Escarpment (BRE), the fairly sharp boundary between high and low topographic relief in the Appalachians (Gallen et al., 2013). Other studies have noted a change in lithospheric structure at the BRE and attributed this to delamination (Wagner et al. 2012, Gallen et al. 2013). If lithospheric thickness is shown to decrease in this area, this structure might be indicative of delamination beneath the southern Appalachian orogen (Sacks and Secor, 1990). More analysis is needed before this structure can be fully characterized.

7. Conclusion

SESAME experiment Rayleigh wave tomography shows that the area around the Suwannee suture has a LAB depth that is fairly typical of continental regions (Fischer et al., 2010). Model LAB depths appear to range from ~125 km to ~150 km (Figure 6.5). The LAB appears to be relatively consistent across the suture, rift basins, and areas with low phase and shear velocities. Generally consistent lithospheric thicknesses across the suture and rift areas may indicate that lithospheric delamination did not occur in this area, contrary to earlier models (e.g. Sacks and Secor, 1990). Zones of low velocity around northern Florida persist through much of the depth range of the mantle lithosphere. These zones are most likely related to subduction related intrusions in the overriding Suwannee terrane that cause a difference in hydration in low velocity areas relative to surrounding mantle lithosphere. Furthermore, we have identified southward dipping structures that occur in the Suwannee suture zone. As such, our study reinforces previous models that indicate Laurentia subducted beneath Suwannee during accretion (McBride and Nelson 1988, Nelson et al. 1985a) and provides evidence against the argument that Suwannee was accreted along a transpressional margin (Mueller et al., 2013).

In addition to improving the characterization of the upper mantle near Suwannee, we have identified a zone of low velocities in the mantle significantly north of the suture along the southern margin of the Appalachians. This feature appears to occur within the lithospheric mantle, but the LAB transition is not clear beneath this location (Figure 6.4). The significance of this structure has yet to be determined, and ongoing studies will likely shed light on this interesting feature.

Figures

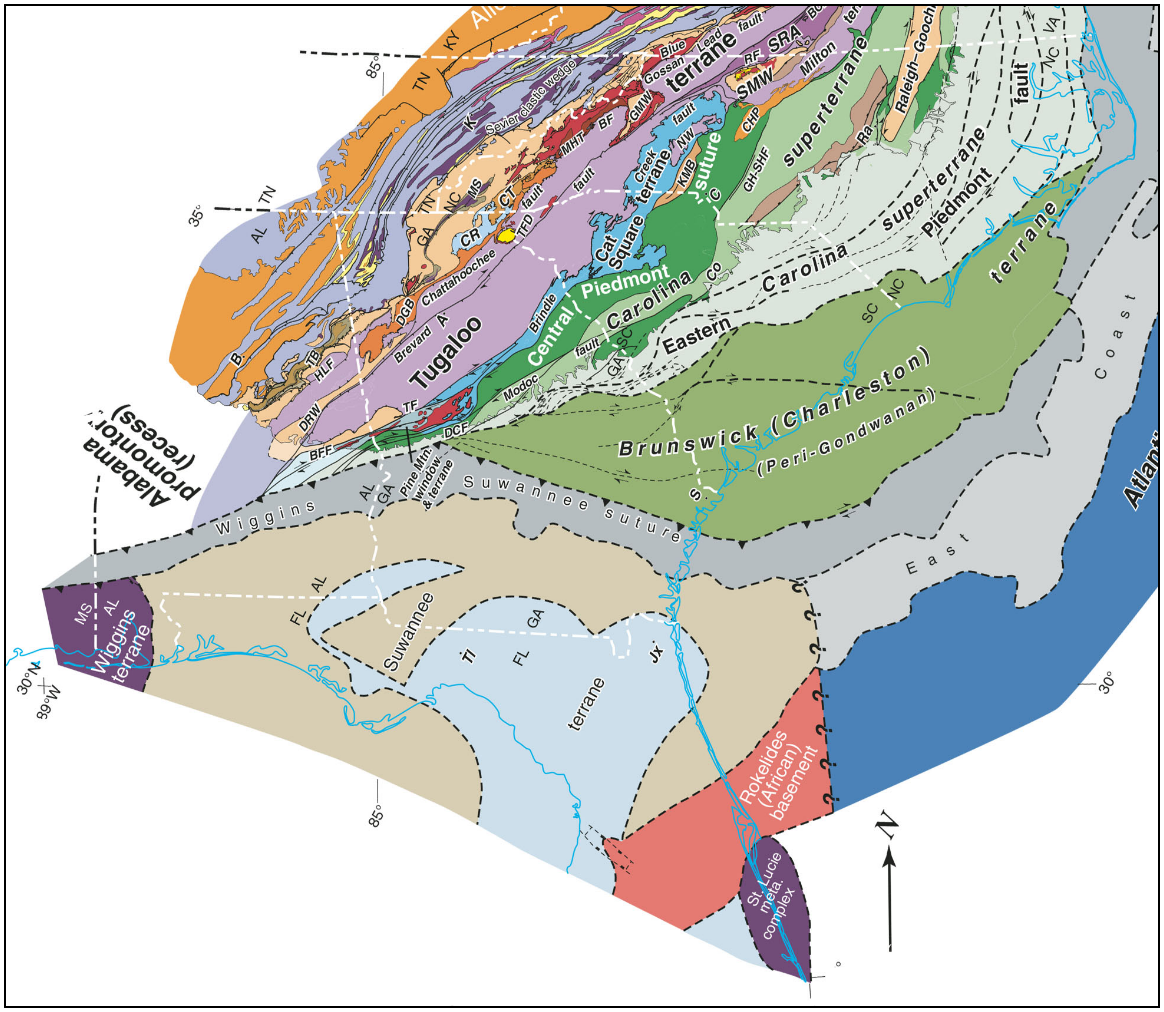

Figure 2.1 Geologic map of the southeastern United States. Tan colored units south of the Suwannee suture are areas affected by Mesozoic rifting (Hatcher, 2010). Figure taken from Hatcher (2010).

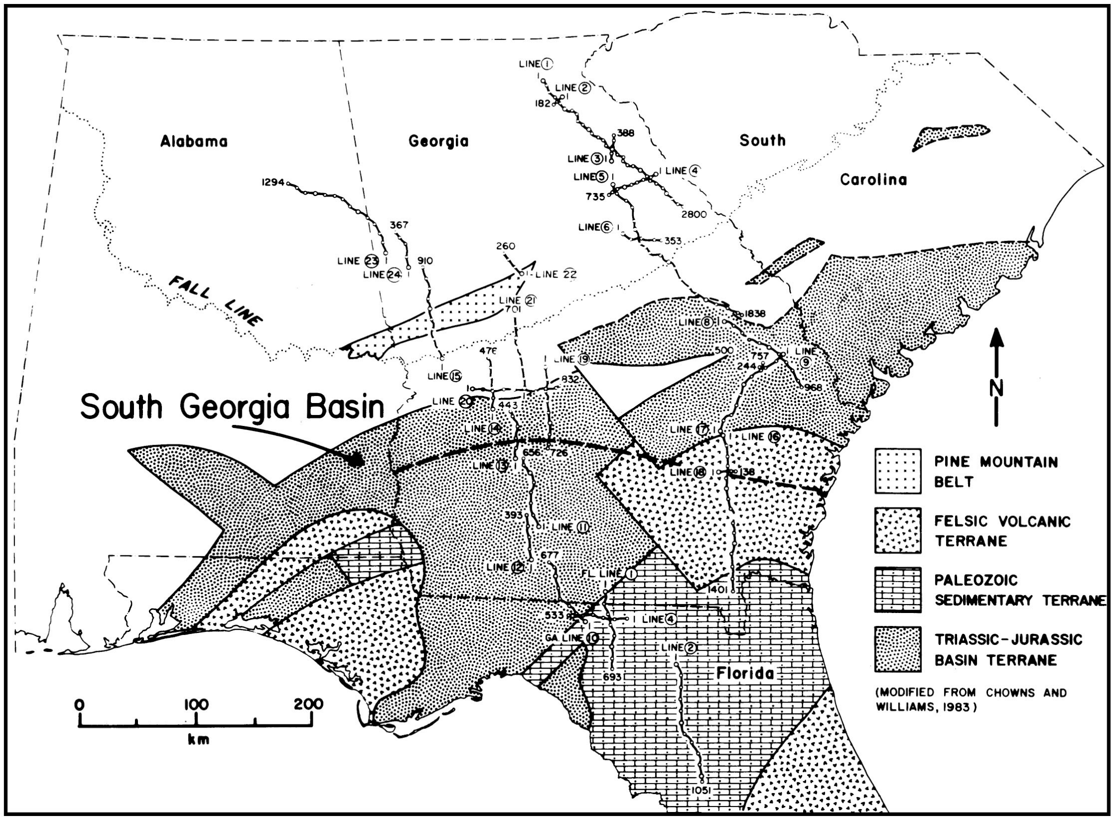

Figure 2.2 Geologic map of Suwannee suture area depicting the spatial extent of Mesozoic rift basins as well as the location of the Suwannee suture (dashed line). Figure is from McBride and Nelson (1988).

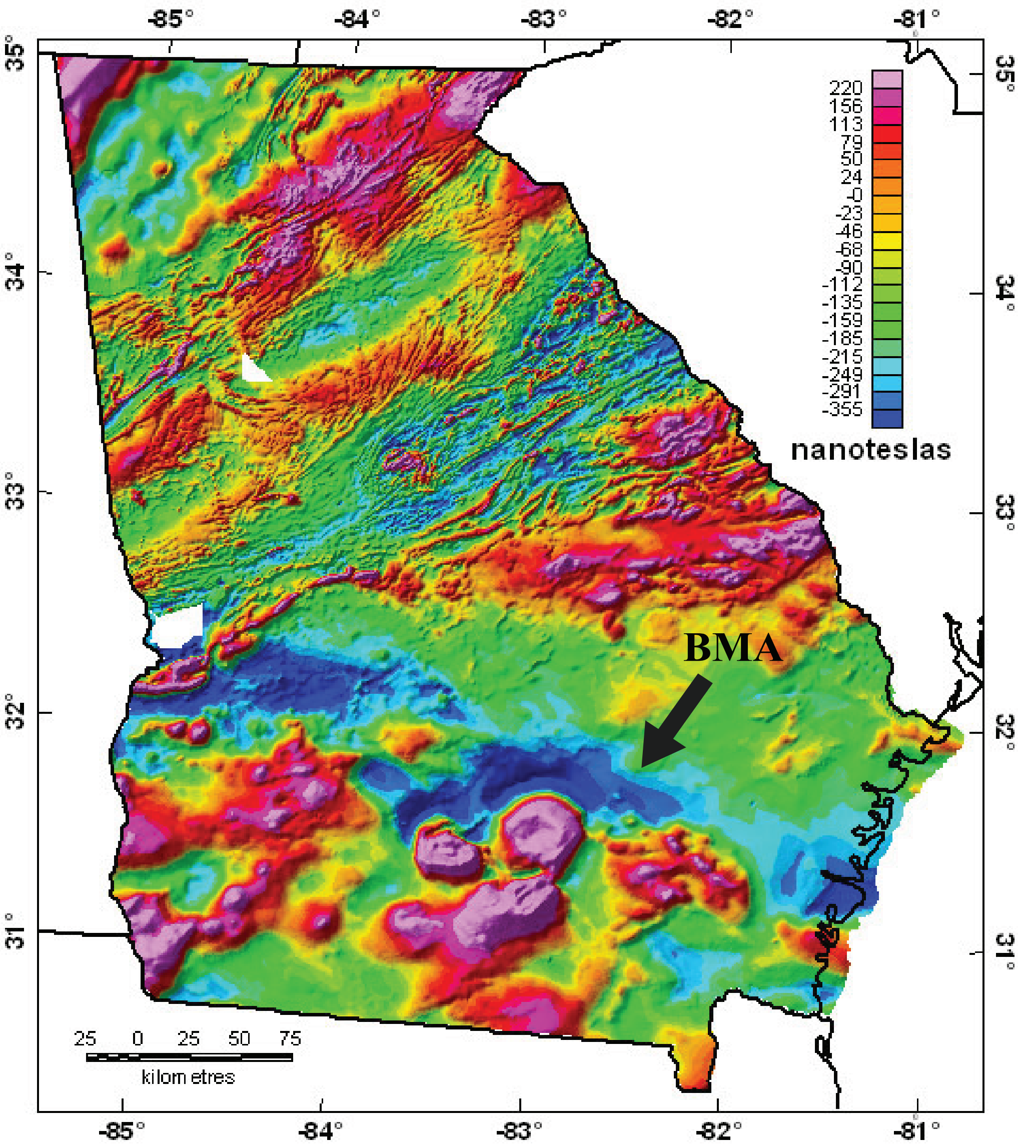

Figure 2.3 Aeromagnetic map of the southeastern United States from the USGS (Daniels, 2001). Reds indicate high magnetism and blues indicate low magnetism. The Brunswick Magnetic Anomaly is indicated by BMA (McBride and Nelson, 1988).

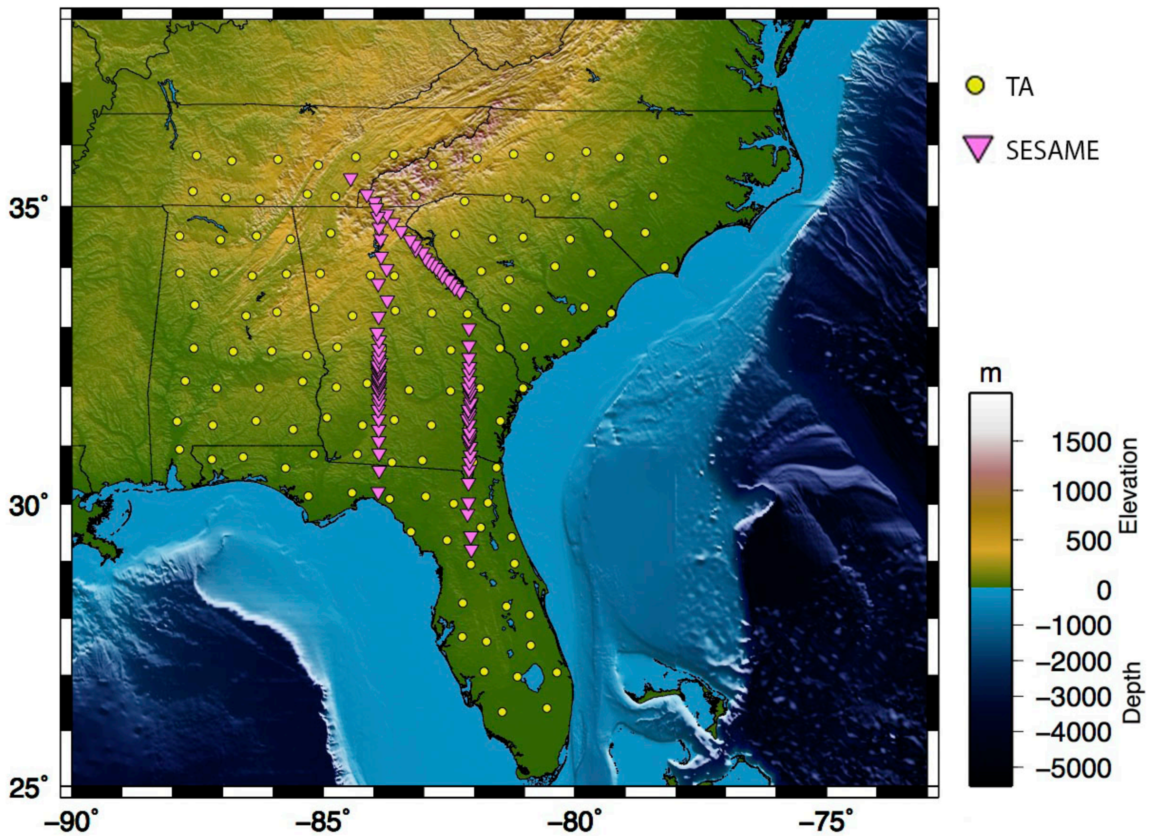

Figure 3.1 Map of study area with stations. Purple triangles are SESAME stations. Yellow dots are TA stations.

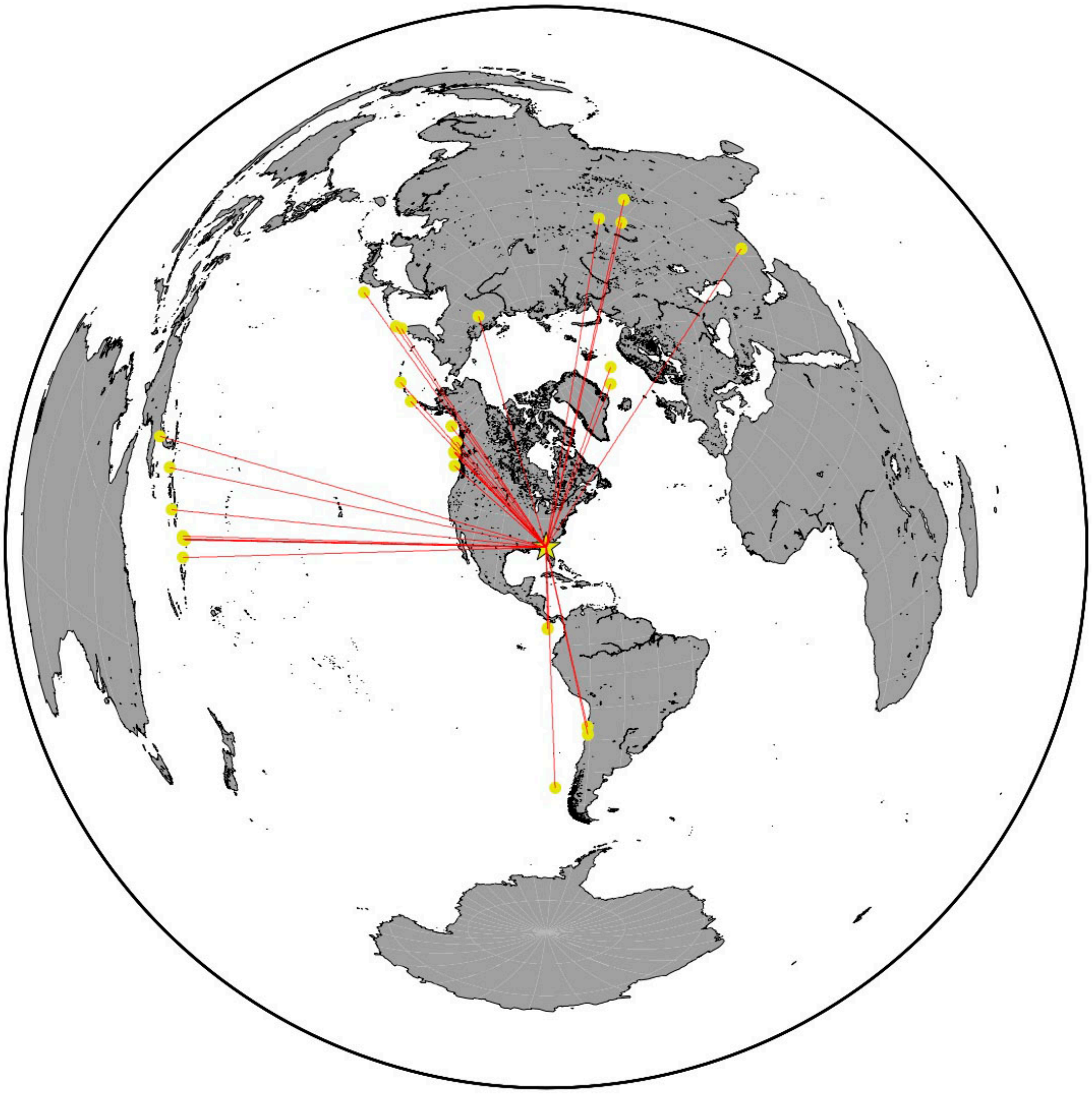

Figure 3.2 Map of the 32 Rayleigh wave arrivals used for this study, including back azimuths. While azimuthal coverage was relatively well distributed, we lacked a substantial group of arrivals from the southwest and southeast.

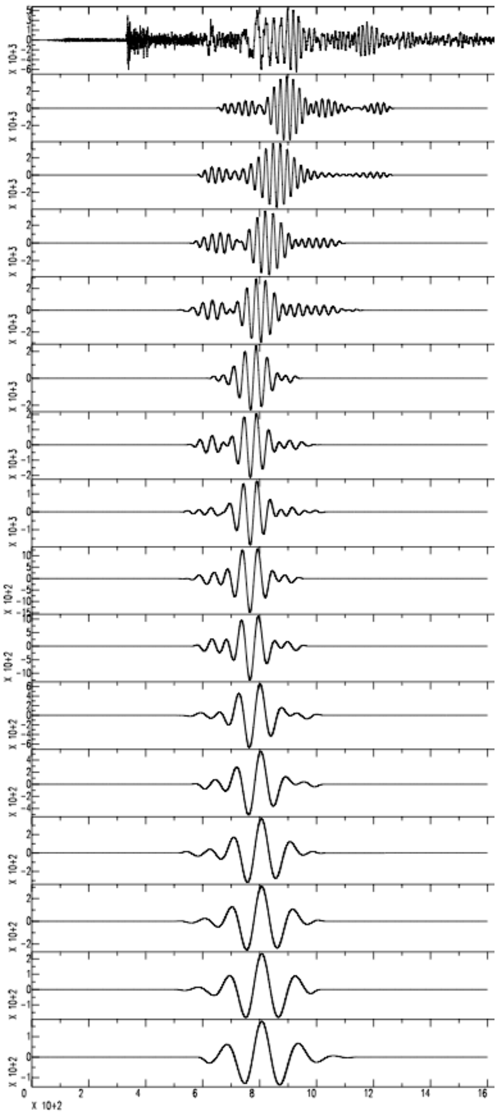

Figure 3.3 Example of Rayleigh wave arrivals from an event occurring on 156, 2012. The top section shows an unfiltered seismogram. The following sections show filtered and cut seismograms for periods ranging from 22.2 s to 143 s (top to bottom). Note that we were later limited to using periods ≥ 33 s for the inversion due to signal quality issues.

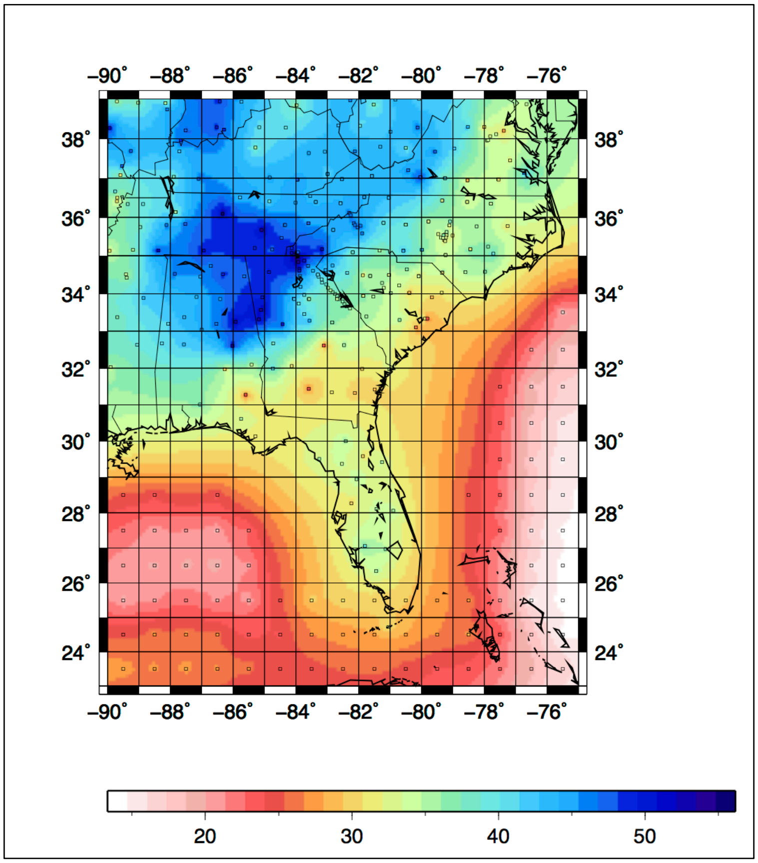

Figure 4.1 Map of Moho depths (in km) used for our starting model.

Depth Range (km):	Number of Layers:	Layer Thickness (km):
1-100	10	10
100-145	3	15
145-265	4	30
265-305	1	40
305-355	1	50
355-595	4	60

Table 4.1 Summary of layers defined for the shear wave velocity inversion.

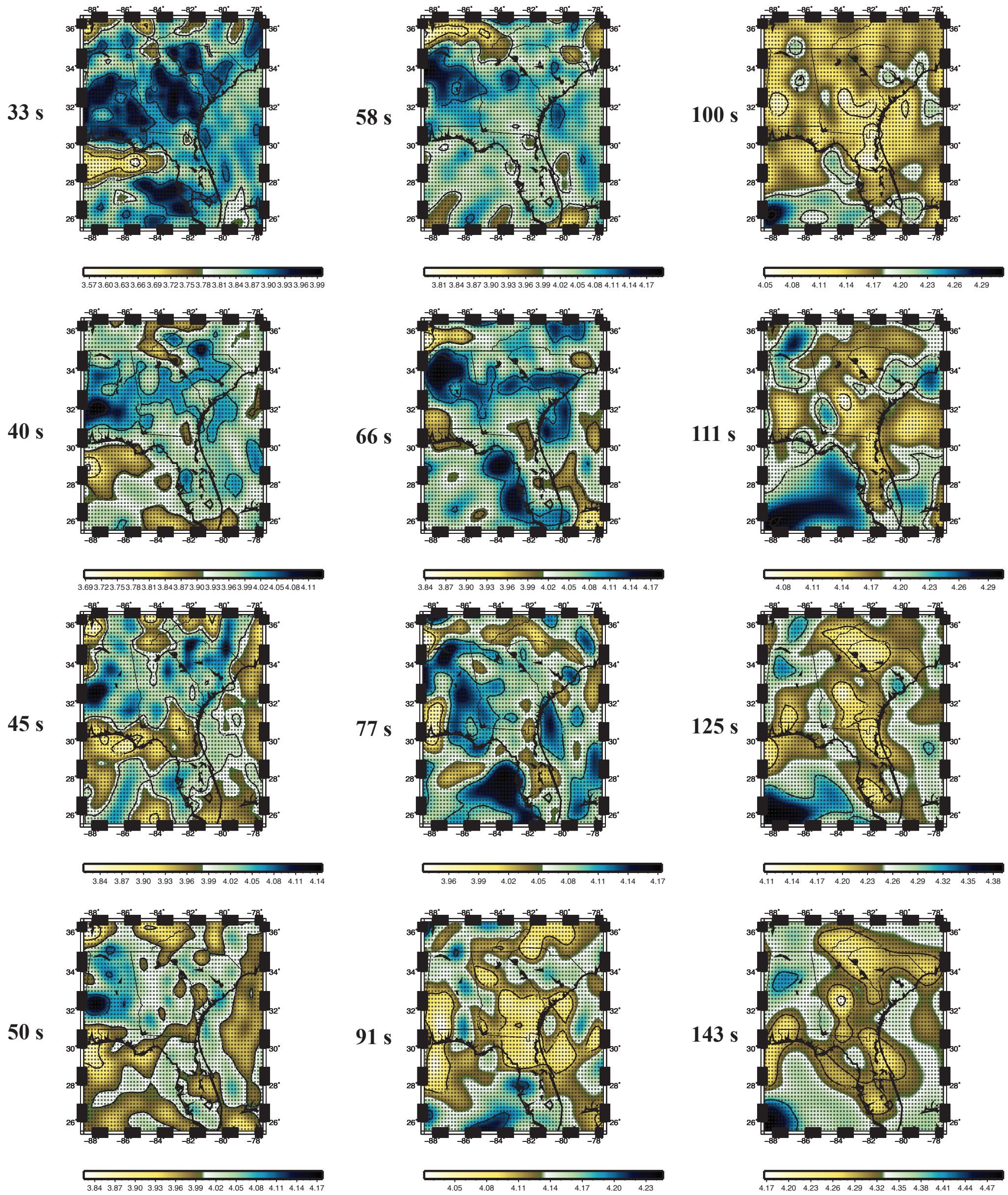

Figure 5.1a Maps of absolute phase velocity in km/s for periods spanning 33-143 s. Blues indicate higher phase velocities and yellows indicate lower phase velocities.

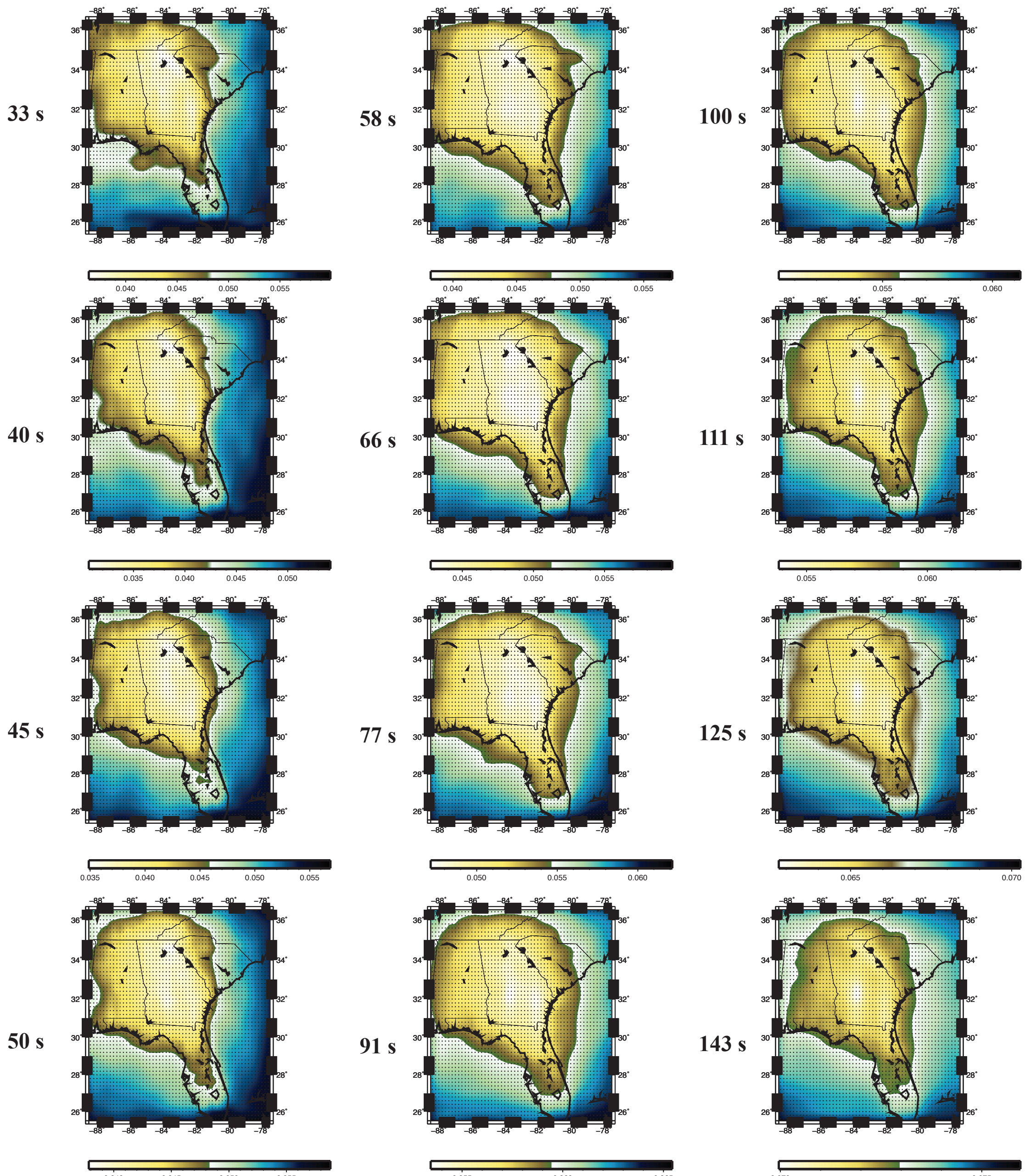

Figure 5.1b Maps of standard deviation for calculated phase velocities. Blues and yellows indicate higher and lower standard deviation values, respectively.

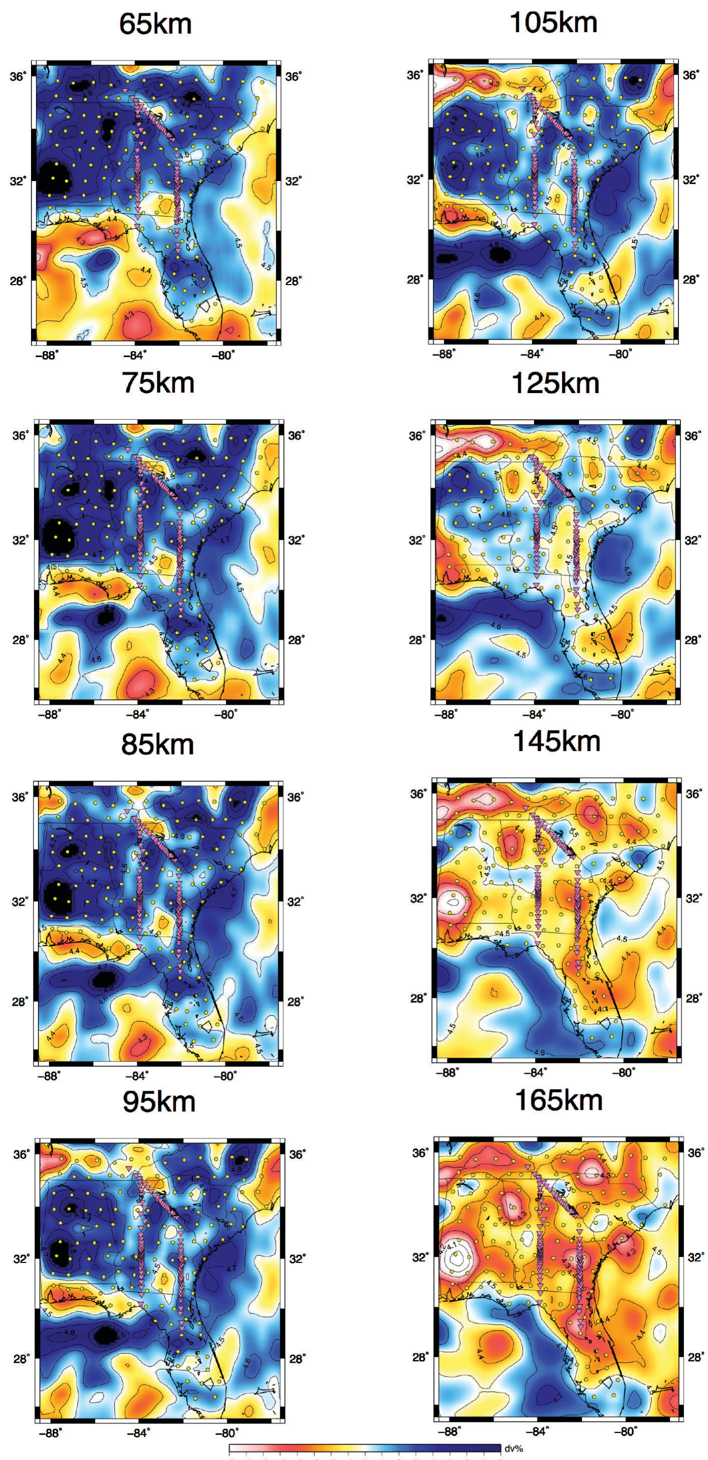

Figure 5.2 Maps of % deviation of shear wave velocities (dVs) from our starting model for 8 depths spanning 65-165 km. Contours indicate absolute shear wave velocities in km/s. Green circles indicate TA stations and purple triangles indicate SESAME stations.

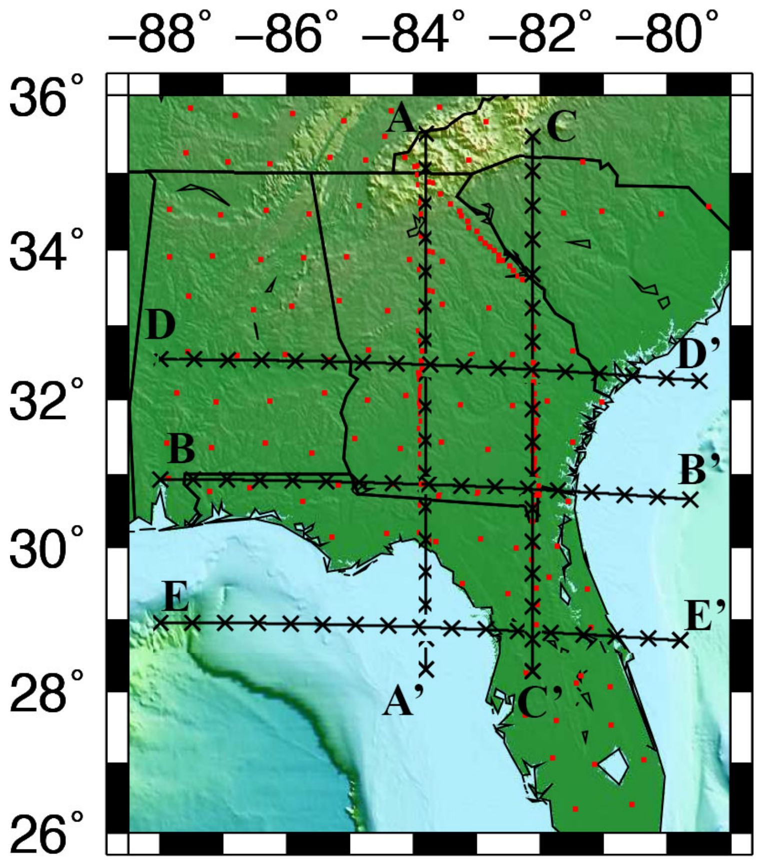

Figure 5.3 Map indicating the locations of cross section lines A-E. X marks are spaced in 50 km increments along strike.

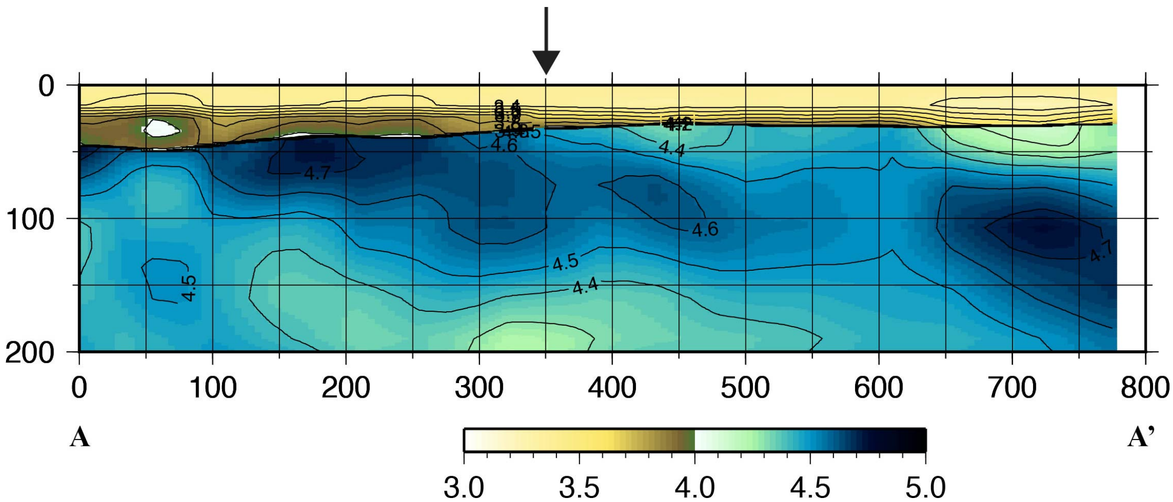

Figure 5.4 Cross section of absolute shear wave velocity (km/s) along line A-A'. Depth and along strike distance are in km. The gray line demarcates where we defined the Moho in our starting model (Figure 4.1). The black arrow indicates the approximate location of the Suwannee suture as shown by Hatcher (2010).

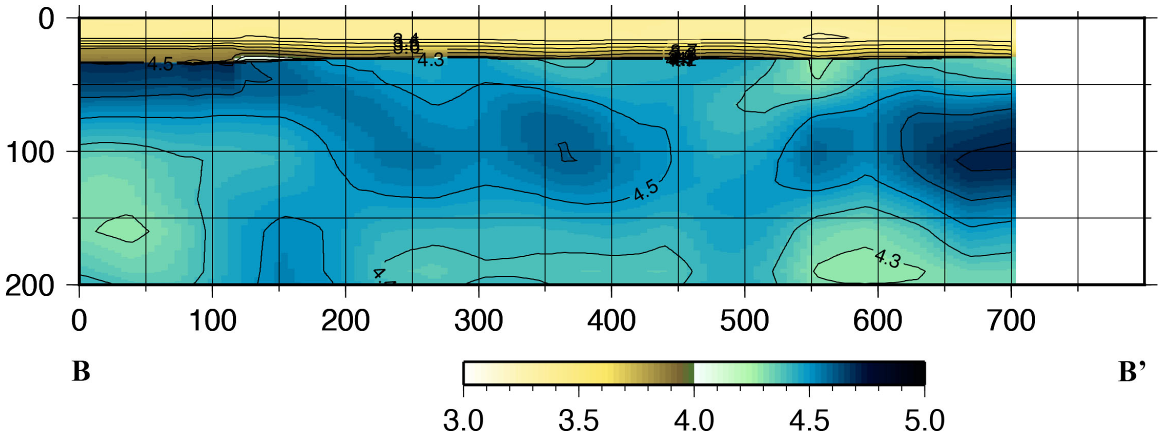

Figure 5.5 Cross section of absolute shear wave velocity (km/s) along line B-B'. Depth and along strike distance are in km. The gray line demarcates where we defined the Moho in our starting model (Figure 4.1).

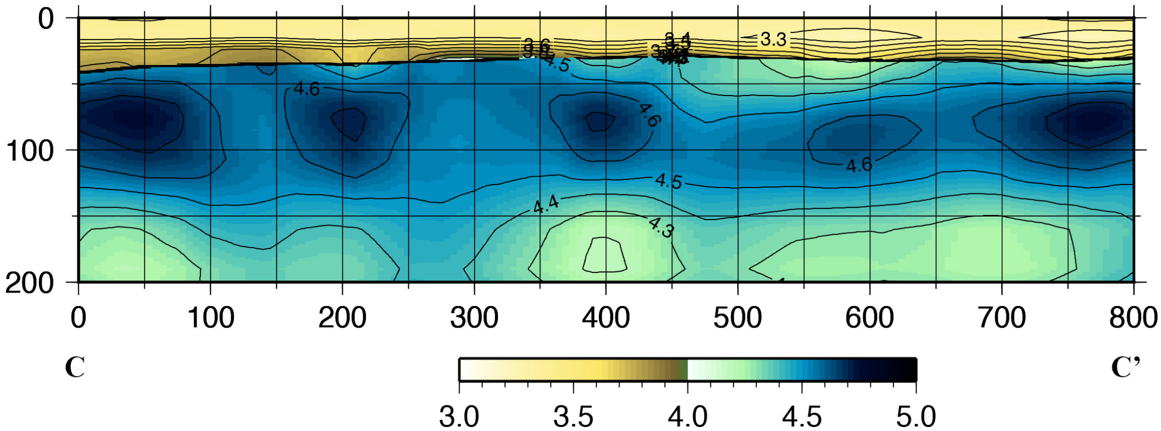

Figure 5.6 Cross section of absolute shear wave velocity (km/s) along line C-C'. Depth and along strike distance are in km. The gray line demarcates where we defined the Moho in our starting model (Figure 4.1).

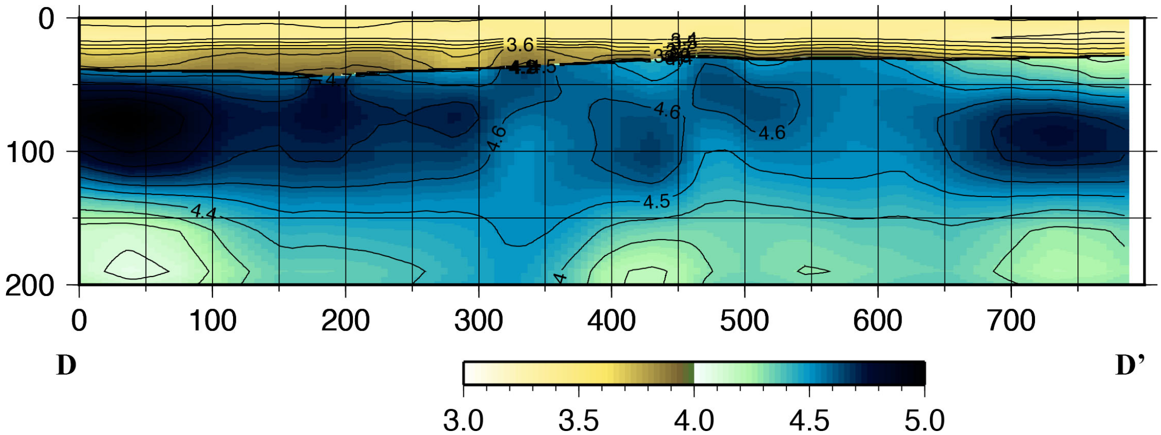

Figure 5.7 Cross section of absolute shear wave velocity (km/s) along line D-D'. Depth and along strike distance are in km. The gray line demarcates where we defined the Moho in our starting model (Figure 4.1).

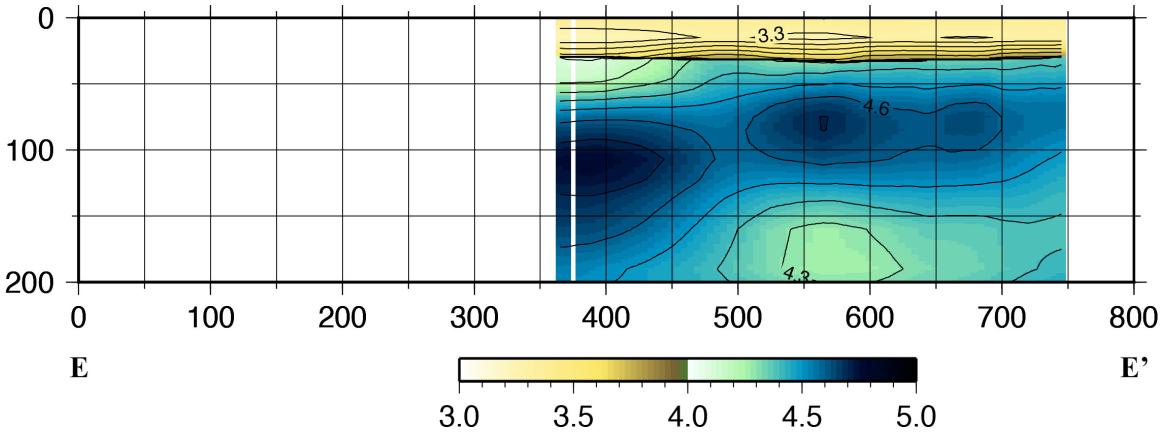

Figure 5.8 Cross section of absolute shear wave velocity (km/s) along line E-E’. Depth and along strike distance are in km. The gray line demarcates where we defined the Moho in our starting model (Figure 4.1).

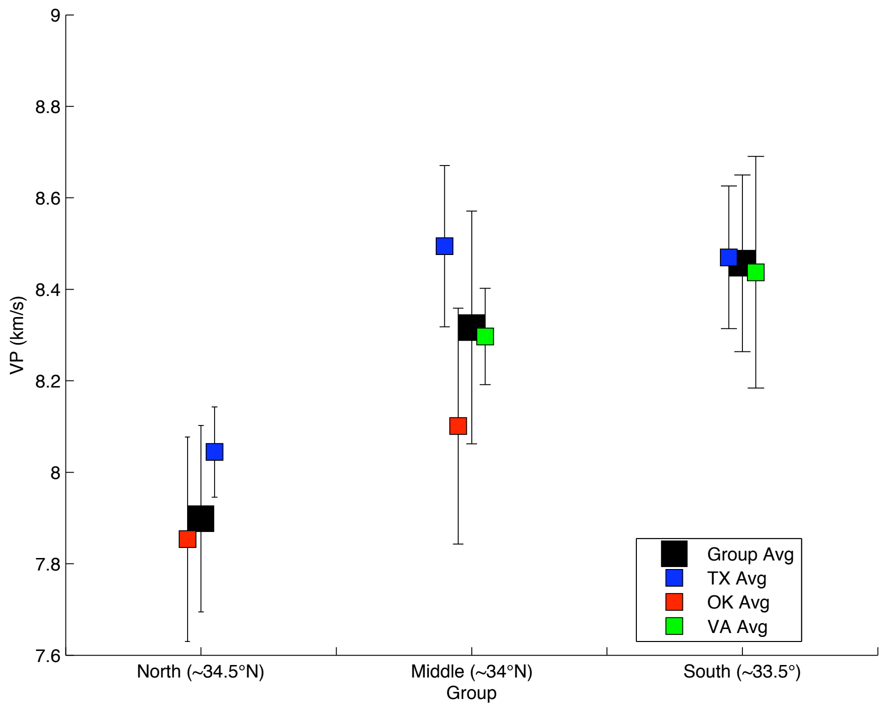

Figure 5.9 Crustal P-wave velocities (Vp) from Pn arrivals that were recorded by the SESAME array. Velocities are grouped by latitude. A distinct drop in Vp is visible between 34-34.5ºN (Julia MacDougall, personal communication, April 11, 2014).

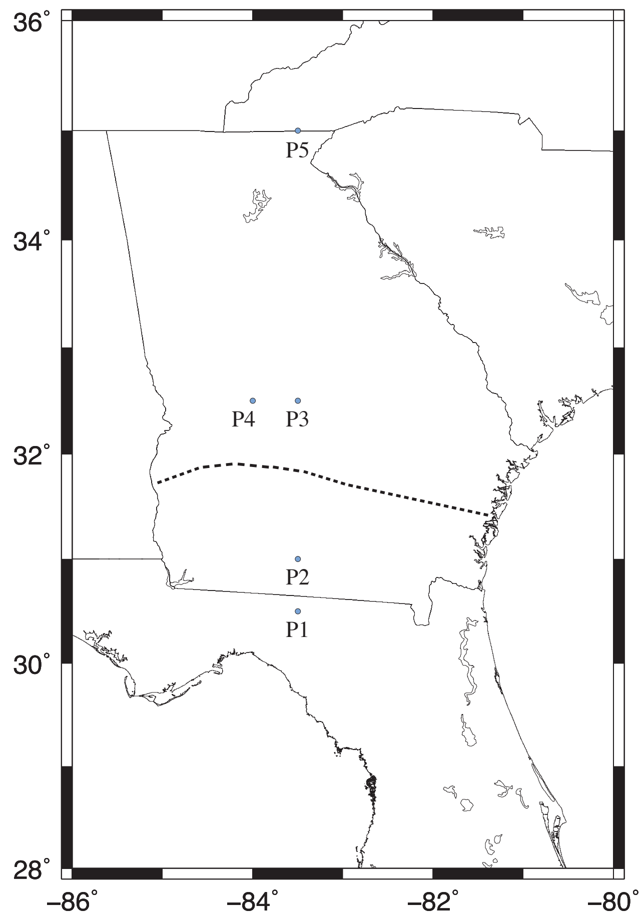

Figure 6.1 Map of 1D profile locations. The dashed line indicates the approximate location of the Suwannee suture as defined by McBride and Nelson (1988).

.

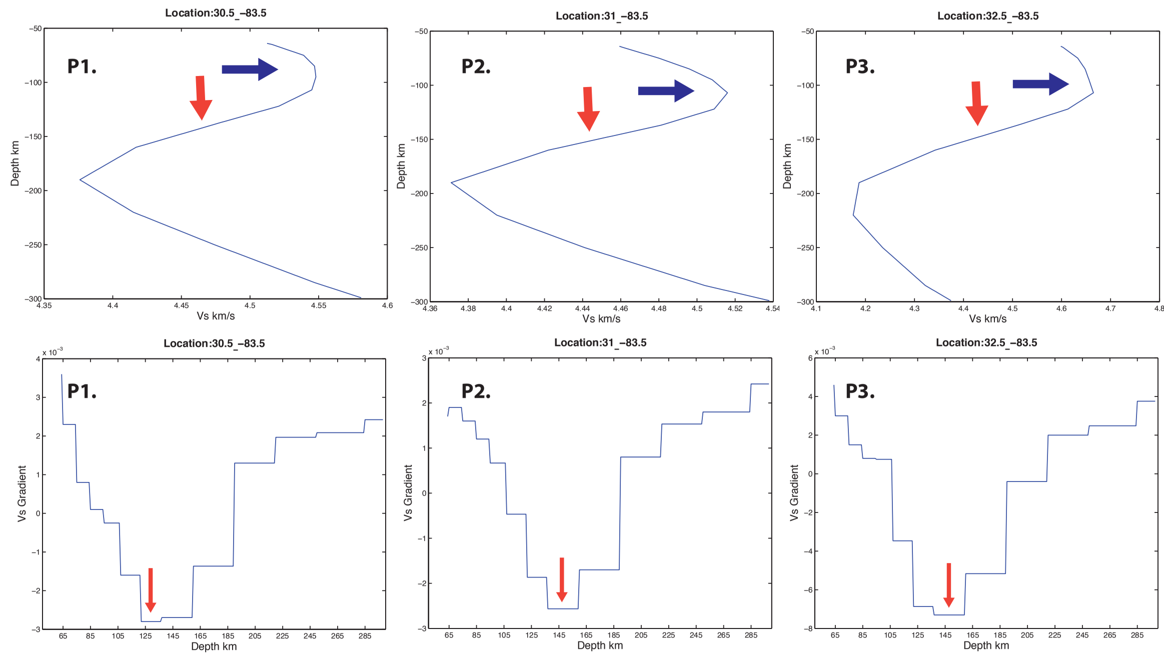

Figure 6.2 (Top) One dimensional profiles of shear wave velocities at points P1-P3. (Bottom) Gradient for shear wave velocity curves with increasing depth. Blue arrows indicate the high velocity, upper mantle "lid". Red arrows indicate the estimated location of the LAB.

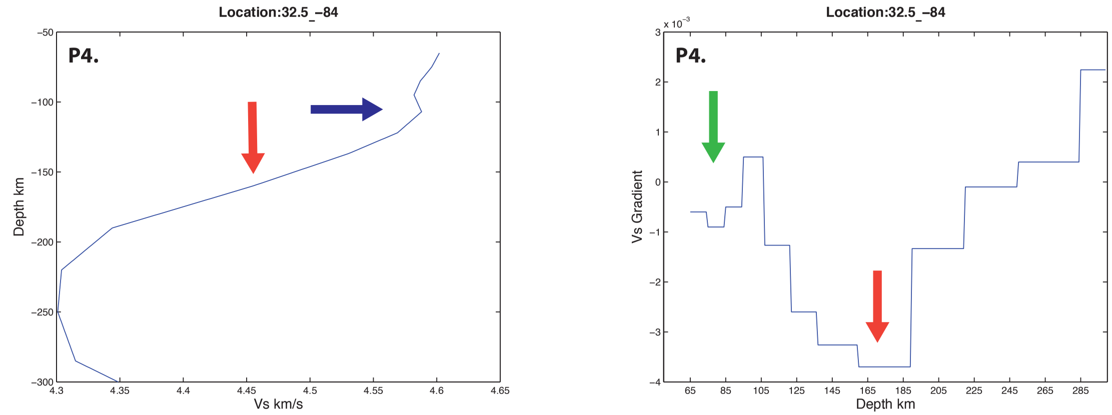

Figure 6.3 1-D shear wave velocity profile (left) and gradient (right). The blue arrow indicates the high velocity, upper mantle "lid" and the red arrows indicate the estimated depth of the LAB. The green arrow shows the zone of decreasing velocities above the LAB that may correspond to the negative Sp phase Abt et al. (2010) observe.

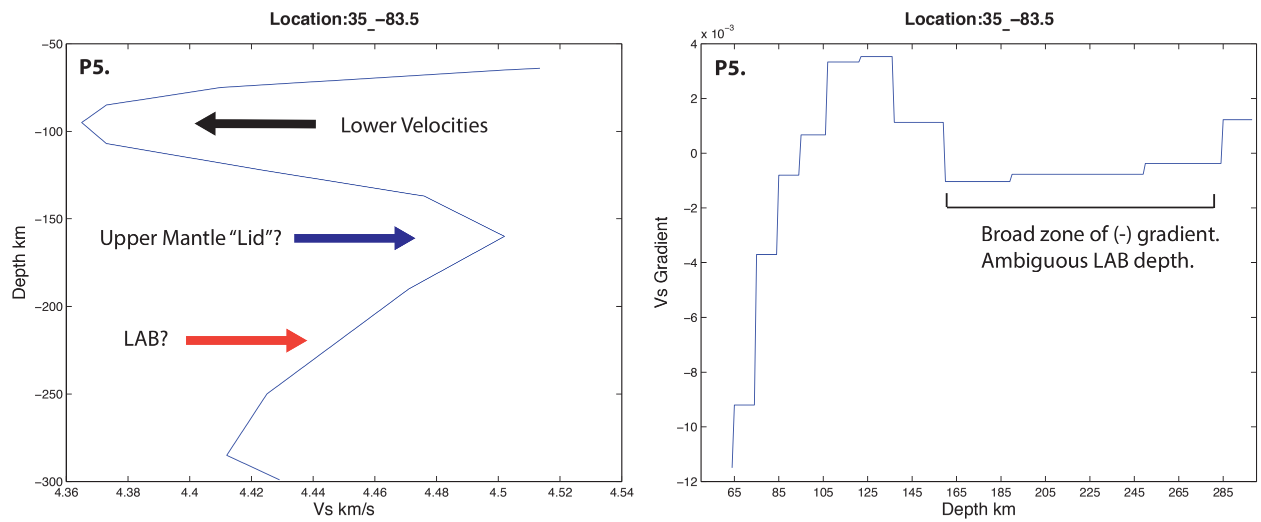

Figure 6.4 Example of a 1-D shear wave velocity profile beneath the southern Appalachians (left) and corresponding gradient (right). There is a broad zone of decreasing velocity that spans ~150-285km, and the LAB is ambiguous. There is also a zone of low velocities occuring below 100km depth that corresponds to low velocity anomalies in Figure 5.2.

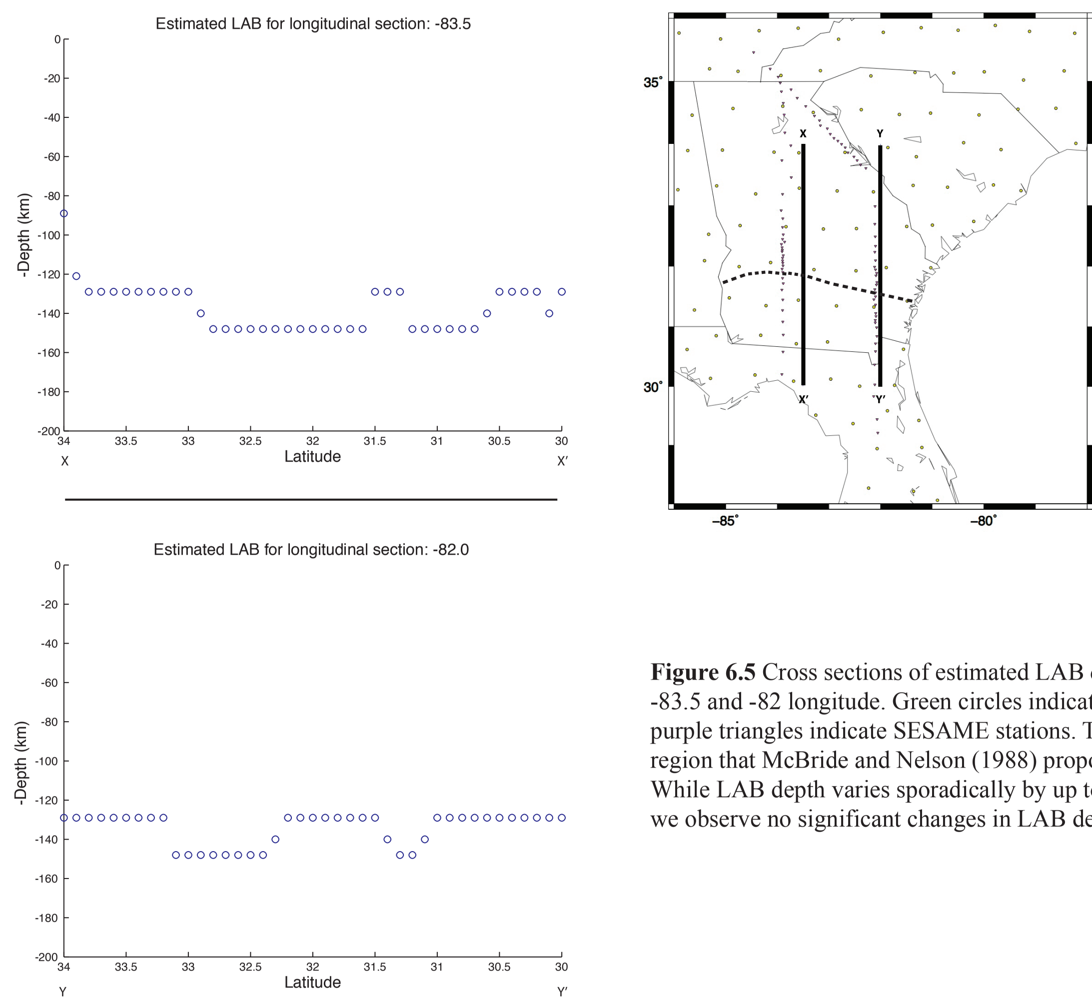

Figure 6.5 Cross sections of estimated LAB depth for lines along -83.5 and -82 longitude. Green circles indicate TA seismic stations and purple triangles indicate SESAME stations. The dashed line indicates the region that McBride and Nelson (1988) propose as the Suwannee suture. While LAB depth varies sporadically by up to ~30 km across the study area, we observe no significant changes in LAB depth across the suture zone.

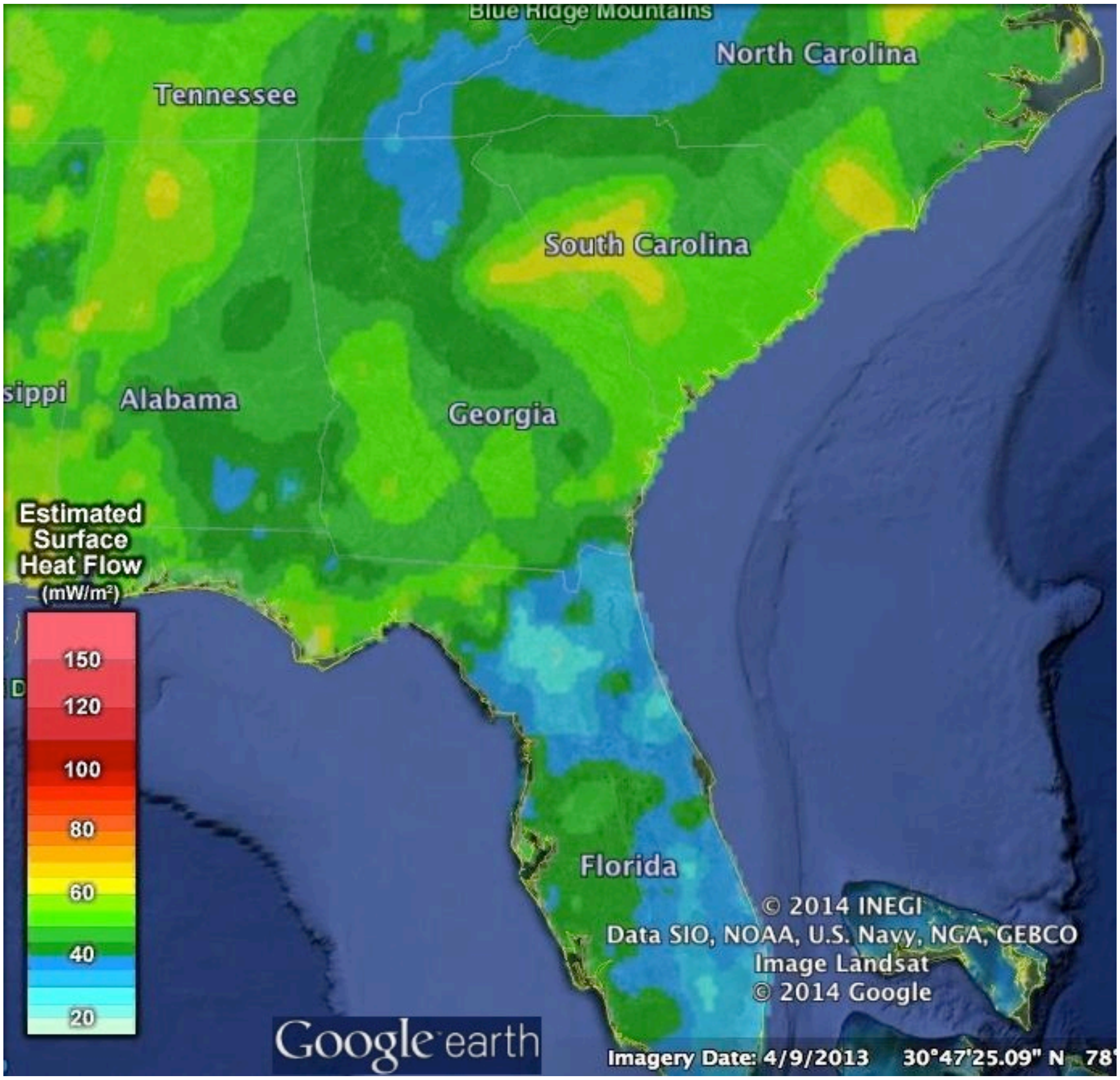

Figure 6.6 Estimated surface heat flow for the Suwannee suture region. Image provided by the Google Enhanced Geothermal Systems Potential project (http://www.google.org/egs/) and is based on Blackwell et al. (2006).

References

Abt, David L., et al. "North American lithospheric discontinuity structure imaged by Ps and Sp receiver functions." *Journal of Geophysical Research: Solid Earth (1978–2012)* 115.B9 (2010).

Blackwell, David D., Petru T. Negraru, and Maria C. Richards. "Assessment of the enhanced geothermal system resource base of the United States." *Natural Resources Research* 15.4 (2006): 283-308.

Blackwell, David D., John L. Steele, and L. S. Carter. "Heat flow patterns of the North American continent: A discussion of the DNAG geothermal map of North America." *Neotectonics of North America* 1 (1991): 423-437.

Chowns, T. M., and C. T. Williams. *Pre-Cretaceous rocks beneath the Georgia Coastal Plain: regional implications*. US Department of the Interior, Geological Survey, 1983.

Christensen, Nikolas I. "Ophiolites, seismic velocities and oceanic crustal structure." *Tectonophysics* 47.1 (1978): 131-157.

Cook, Frederick A., and Kris Vasudevan. "Reprocessing and enhanced interpretation of the initial COCORP Southern Appalachians traverse." *Tectonophysics* 420.1 (2006): 161-174.

Cook, Frederick A., et al. "Thin-skinned tectonics in the crystalline southern Appalachians; COCORP seismic-reflection profiling of the Blue Ridge and Piedmont." *Geology* 7.12 (1979): 563-567.

Cramer, Fritz H. "Position of the North Florida Lower Paleozoic Block in Silurian time phytoplankton evidence." *Journal of Geophysical Research* 76.20 (1971): 4754-4757.

Dallmeyer, R. D. "40Ar/39Ar age of detrital muscovite within Lower Ordovician sandstone in the coastal plain basement of Florida: Implications for west African terrane linkages." *Geology* 15.11 (1987): 998-1001.

Dallmeyer, R. D., M. Caen-Vachette, and M. Villeneuve. "Emplacement age of post-tectonic granites in southern Guinea (West Africa) and the peninsular Florida subsurface: Implications for origins of southern Appalachian exotic terranes." *Geological Society of America Bulletin* 99.1 (1987): 87-93.

Daniels, David. *Georgia Merged Aeromagnetic Anomaly Map*. 2001. Map. USGSWeb. 13 Apr 2014. <http://pubs.usgs.gov/of/2001/of01-106/>.

Daniels, David Lee, Isidore Zietz, and Peter Popenoe. *Distribution of subsurface lower Mesozoic rocks in the southeastern United States, as interpreted from regional aeromagnetic and gravity maps*. US Department of the Interior, Geological Survey, 1983.

Drury, M. R., et al. "Emplacement of deep upper-mantle rocks into cratonic lithosphere by convection and diapiric upwelling." *Journal of Petrology* 42.1 (2001): 131-140.

Eaton, David W., et al. "The elusive lithosphere–asthenosphere boundary (LAB) beneath cratons." *Lithos* 109.1 (2009): 1-22.

Engelder, Terry, and Amy Whitaker. "Early jointing in coal and black shale: Evidence for an Appalachian-wide stress field as a prelude to the Alleghanian orogeny." *Geology* 34.7 (2006): 581-584.

Faul, Ulrich H., and Ian Jackson. "The seismological signature of temperature and grain size variations in the upper mantle." *Earth and Planetary Science Letters* 234.1 (2005): 119-134.

Fischer, Karen M., et al. "The lithosphere-asthenosphere boundary." *Annual Review of Earth and Planetary Sciences* 38 (2010): 551-575.

Ford, Heather A., et al. "The lithosphere–asthenosphere boundary and cratonic lithospheric layering beneath Australia from Sp wave imaging." *Earth and Planetary Science Letters* 300.3 (2010): 299-310.

Forsyth, Donald W., and Aibing Li. "Array analysis of two-dimensional variations in surface wave phase velocity and azimuthal anisotropy in the presence of multipathing interference." *Geophysical Monograph Series* 157 (2005): 81-97.

Gallen, Sean F., Karl W. Wegmann, and D. R. Bohnenstiehl. "Miocene rejuvenation of topographic relief in the southern Appalachians." *GSA Today* 23.2 (2013): 4-10.

Hatcher Jr, Robert D. "The Appalachian orogen: A brief summary." *From Rodinia to Pangea: The Lithotectonic Record of the Appalachian Region: Geological Society of America Memoir* 206 (2010): 1-19.

Hatcher, Robert D. "Rheological partitioning during multiple reactivation of the Palaeozoic Brevard fault zone, Southern Appalachians, USA." *Geological Society, London, Special Publications* 186.1 (2001): 257-271.

Heatherington, Ann L., Paul A. Mueller, and Joseph L. Wooden. "Alleghanian plutonism in the Suwannee terrane, USA: Implications for late Paleozoic tectonic models." *Geological Society of America Memoirs* 206 (2010): 607-620.

Heatherington, A. L., and P. A. Mueller. "Mesozoic igneous activity in the Suwannee terrane, southeastern USA: petrogenesis and Gondwanan affinities." *Gondwana Research* 6.2 (2003): 296-311.

Hibbard, James P., Cees R. van Staal, and Douglas W. Rankin. "Comparative analysis of the geological evolution of the northern and southern Appalachian orogen: Late Ordovician-Permian." *From Rodinia to Pangea: The Lithotectonic Record of the Appalachian Region: Geological Society of America Memoir* 206 (2010): 51-69.

Hynes, Andrew. "Two-stage rifting of Pangea by two different mechanisms." *Geology* 18.4 (1990): 323-326.

Jackson, Ian, et al. "Grain-size-sensitive seismic wave attenuation in polycrystalline olivine." *Journal of Geophysical Research: Solid Earth (1978–2012)* 107.B12 (2002): ECV-5.

Karato, Shun-ichiro. "Mapping water content in the upper mantle." *Geophysical Monograph Series* 138 (2003): 135-152.

Karato, Shun-ichiro, and Haemyeong Jung. "Water, partial melting and the origin of the seismic low velocity and high attenuation zone in the upper mantle." *Earth and Planetary Science Letters* 157.3-4 (1998): 193-207.

Kohlstedt, David L., and Mark E. Zimmerman. "Rheology of partially molten mantle rocks." *Annual Review of Earth and Planetary Sciences* 24.1 (1996): 41-62.

Kennett , BL N_, and E. R. Engdahl. "Travel times for global earthquake location and phase identification." *Geophysical Journal International* 105.2 (1991): 429-465.

Laske, Gabi, et al. "Update on CRUST1. 0—a 1-degree global model of Earth's crust." *EGU general assembly* (2013).

Li, Aibing. "Shear wave model of southern Africa from regional Rayleigh wave tomography with 2-D sensitivity kernels." *Geophysical Journal International* 185.2 (2011): 832-844.

MacDougall, Julia. "Vp Velocities". 11 April 2014. Email.

McBride, J. H., K. D. Nelson, and L. D. Brown. "Early Mesozoic basin structure and tectonics of the southeastern United States as revealed from COCORP reflection data and the relation to Atlantic rifting." (1987): 173-184.

McBride, J. H., and K. D. Nelson. "Integration of COCORP deep reflection and magnetic anomaly analysis in the southeastern United States: Implications for origin of the Brunswick and East Coast magnetic anomalies." *Geological Society of America Bulletin* 100.3 (1988): 436-445.

Morgan, Jason Phipps, and Donald W. Forsyth. "Three-dimensional flow and temperature perturbations due to a transform offset: Effects on oceanic crustal and upper mantle structure." *Journal of Geophysical Research: Solid Earth (1978–2012)* 93.B4 (1988): 2955-2966.

Moore, Vernon M., and David V. Wiltschko. "Syncollisional delamination and tectonic wedge development in convergent orogens." *Tectonics* 23.2 (2004).

Murphy, J. Brendan. "Igneous rock associations 7. Arc magmatism I: relationship between subduction and magma genesis." *Geoscience Canada* 33.4 (2006).

Nelson, K. D., et al. "New COCORP profiling in the southeastern United States. Part I: Late Paleozoic suture and Mesozoic rift basin." *Geology* 13.10 (1985): 714-718.

Nelson, K. D., et al. "New COCORP profiling in the southeastern United States. Part II: Brunswick and east coast magnetic anomalies, opening of the north-central Atlantic Ocean." *Geology* 13.10 (1985): 718-721.

Nomade, S., et al. "Chronology of the Central Atlantic Magmatic Province: implications for the Central Atlantic rifting processes and the Triassic–Jurassic biotic crisis." *Palaeogeography, Palaeoclimatology, Palaeoecology* 244.1 (2007): 326-344.

O'Reilly, Suzanne Y., and W. L. Griffin. "The continental lithosphere–asthenosphere boundary: Can we sample it?." *Lithos* 120.1 (2010): 1-13.

Palomeras, I., et al. "Finite‐frequency Rayleigh wave tomography of the western Mediterranean: Mapping its lithospheric structure." *Geochemistry, Geophysics, Geosystems* (2014).

Parker, E. Horry, et al. "Crustal evolution across the southern Appalachians: Initial results from the SESAME broadband array." *Geophysical Research Letters* 40.15 (2013): 3853-3857.

Peacock, Simon A. "Fluid processes in subduction zones." *Science* 248.4953 (1990): 329-337.

Peavy, Samuel T., et al. "Contrasts in Tectonic style of the Central and Southern Appalachians, United States: Insights from seismic reflection data." *Journal of Geodynamics* 37.3 (2004): 633-655.

Pojeta, John, Jiří Kříž, and Jean Milton Berdan. *Silurian-Devonian pelecypods and Paleozoic stratigraphy of subsurface rocks in Florida and Georgia and related Silurian pelecypods from Bolivia and Turkey*. US Government Printing Office, 1976.

Sacks, Paul E., and Donald T. Secor. "Delamination in collisional orogens." *Geology* 18.10 (1990): 999-1002.

Secor, Donald T., Arthur W. Snoke, and R. David Dallmeyer. "Character of the Alleghanian orogeny in the southern Appalachians: Part III. Regional tectonic relations." *Geological Society of America Bulletin* 97.11 (1986): 1345-1353.

Shearer, Peter M. *Introduction to seismology*. Cambridge University Press, 2009.

Storey, Bryan C. "The role of mantle plumes in continental breakup: case histories from Gondwanaland." *Nature* 377.6547 (1995): 301-308.

Thomas, William A. "The Appalachian-Ouachita rifted margin of southeastern North America." *Geological Society of America Bulletin* 103.3 (1991): 415-431.

Thomas, William A. "Tectonic inheritance at a continental margin." *GSA Today* 16.2 (2006): 4-11.

Wagner, Lara S., Kevin Stewart, and Kathryn Metcalf. "Crustal-scale shortening structures beneath the Blue Ridge Mountains, North Carolina, USA." *Lithosphere* 4.3 (2012): 242-256.

Wagner, Lara, et al. "Detailed three-dimensional shear wave velocity structure of the northwestern United States from Rayleigh wave tomography." *Earth and Planetary Science Letters* 299.3 (2010): 273-284

Weeraratne, Dayanthie S., et al. "Evidence for an upper mantle plume beneath the Tanzanian craton from Rayleigh wave tomography." *Journal of Geophysical Research: Solid Earth (1978–2012)* 108.B9 (2003).

White, Robert, and Dan McKenzie. "Magmatism at rift zones: the generation of volcanic continental margins and flood basalts." *Journal of Geophysical Research: Solid Earth (1978–2012)* 94.B6 (1989): 7685-7729.

Winter, John D. *Principles of igneous and metamorphic petrology*. Vol. 2. New York: Prentice Hall, 2010.

Yang, Yingjie, and Donald W. Forsyth. "Regional tomographic inversion of the amplitude and phase of Rayleigh waves with 2-D sensitivity kernels." *Geophysical Journal International* 166.3 (2006): 1148-1160.